Seasonal variability of water mass distribution in the southeastern Beaufort Sea determined by total alkalinity and delta O-18

B. Lansard, A. Mucci, L. A. Miller, R. W. Macdonald, Y. Gratton

Seasonal variability of water mass distribution in the southeastern Beaufort Sea determined by total alkalinity and $\delta^{18}O$

Bruno Lansard,[1,2] Alfonso Mucci,[1] Lisa A. Miller,[3] Robie W. Macdonald,[3] and Yves Gratton[4]

Received 17 May 2011; revised 17 December 2011; accepted 2 January 2012; published 1 March 2012.

[1] We examined the seasonal variability of water mass distributions in the southeastern Beaufort Sea from data collected between September 2003 and August 2004. Salinity, total alkalinity (TA) and isotopic composition ($\delta^{18}O$) of seawater were used together as tracers of freshwater input, i.e., meteoric water and sea ice meltwater. We used an optimum multiparameter analysis to identify the different water masses, including the Mackenzie River, sea ice melt (SIM), winter polar mixed layer (PML), upper halocline water (UHW) with core salinity of 33.1 psu (Pacific origin) and Atlantic Water. Computed values of CO_2 fugacity in seawater (fCO_2-sw) show that the surface mixed layer (SML) remains mostly undersaturated (328 $\pm$ 55 μatm, n = 552) with respect to the average atmospheric CO_2 concentration (380 $\pm$ 5 μatm) over the study period. The influence of the Mackenzie River ($fCO_{2\text{-SW}} > 500$ μatm) was relatively small in the southeastern Beaufort Sea, and significant fractions were only observed on the inner Mackenzie Shelf. The contribution of sea ice melt ($fCO_{2\text{-SW}} < 300$ μatm) to the SML could reach 30% beyond the shelf break and close to the ice pack in autumn. The density of the PML increased through the winter due to cooling and brine rejection. The winter PML reached a maximum depth of 70 m in late April. The UHW ($fCO_{2\text{-SW}} > 600$ μatm) was usually located between 120 and 180 m depth, but could contribute to the SML during wind-driven upwelling events, in summer and autumn, and during brine-driven eddies, in winter.

Citation: Lansard, B., A. Mucci, L. A. Miller, R. W. Macdonald, and Y. Gratton (2012), Seasonal variability of water mass distribution in the southeastern Beaufort Sea determined by total alkalinity and $\delta^{18}O$, *J. Geophys. Res.*, *117*, C03003, doi:10.1029/2011JC007299.

1. Introduction

[2] One manifestation of change in Arctic climate is an approximately 3°C increase in mean air temperature since the 1970s [*Symon et al.*, 2005; *Intergovernmental Panel on Climate Change*, 2008], and accompanying impacts can already be observed on the terrestrial and marine carbon cycles [*Anderson and Kaltin*, 2001; *Overpeck et al.*, 2005; *Guo et al.*, 2007; *McGuire et al.*, 2009]. Satellite and field observations have revealed a steadily decreasing minimum ice cover in the Arctic Ocean, with recent summer months setting new record lows in terms of ice cover and thickness [*Barber and Hanesiak*, 2004; *Serreze et al.*, 2007; *Howell et al.*, 2009]. A receding ice cover and direct exposure of the air-sea interface will likely result in more efficient CO_2 gas exchange with the atmosphere. In the absence of ice, greater light penetration and an increase in nutrients brought to the euphotic zone by vertical mixing, upwelling and rivers are proposed to enhance primary productivity [*Arrigo et al.*, 2008; *Mundy et al.*, 2009] and the biological CO_2 pump. Hence, under these conditions, the Arctic Ocean will play a more active role in the carbon cycle. However, many factors could counterbalance the potential for the Arctic Ocean to become a greater CO_2 sink [*Bates and Mathis*, 2009; *Cai et al.*, 2010]. For example, increased precipitation and the consequent amplified river runoff are expected to result in a generally greater stratification in the upper ocean and a greater export of dissolved and particulate organic matter to the Arctic shelves [*Benner et al.*, 2004], which could increase the importance of the heterotrophic CO_2 source, relative to photosynthetic drawdown. Because changes in the Arctic might be amplified through numerous feedbacks [*Bates and Mathis*, 2009; *McGuire et al.*, 2009], the role of freshwater inputs (runoff, precipitation and sea ice melt) in establishing the direction and magnitude of CO_2 fluxes in the Arctic Ocean needs to be evaluated.

[3] The Arctic Ocean receives large freshwater inputs from meteoric water (MW; we define this as runoff plus

[1]GEOTOP and Department of Earth and Planetary Sciences, McGill University, Montreal, Quebec, Canada.
[2]Now at Laboratoire d'Études en Géophysique et Océanographie Spatiales, Observatoire Midi-Pyrénées, Toulouse, France.
[3]Centre for Ocean Climate Chemistry, Institute of Ocean Sciences, Fisheries and Oceans Canada, Sidney, British Columbia, Canada.
[4]Centre Eau, Terre et Environnement, Institut National de la Recherche Scientifique, Quebec City, Quebec, Canada.

0148-0227/12/2011JC007299

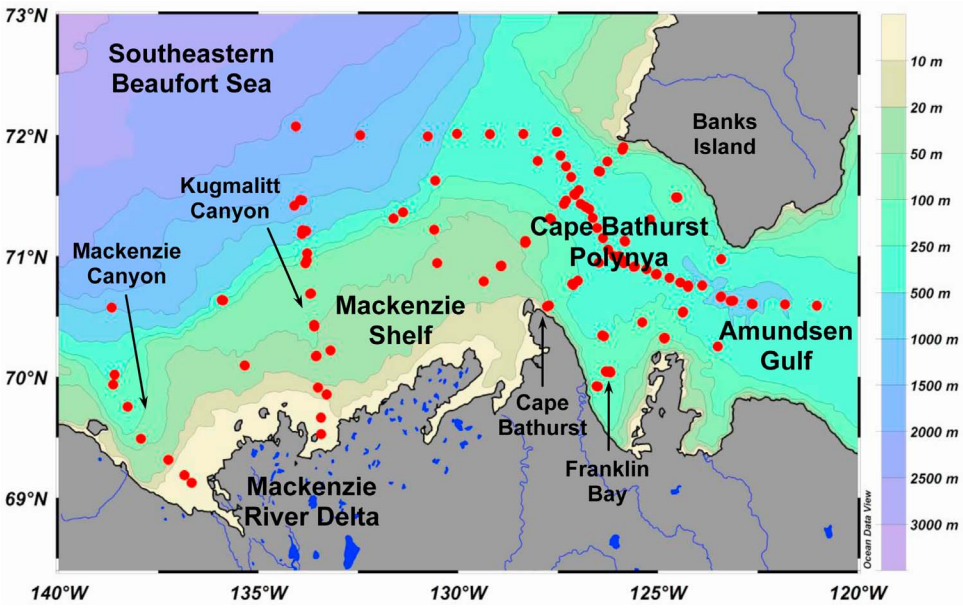

Figure 1. Map of the CASES study area showing the bathymetry and location of the sampling stations covered by the icebreaker CCGS *Amundsen* from September 2003 to August 2004.

precipitation) and sea ice meltwater [*White et al.*, 2007]. Many studies have investigated the freshwater cycle in the Arctic Ocean using geochemical tracers such as the $\delta^{18}O$ of water [*Östlund and Hut*, 1984; *Macdonald et al.*, 1989, 1999b; *Melling and Moore*, 1995; *Ekwurzel et al.*, 2001; *Schlosser et al.*, 2002; *Bauch et al.*, 2005; *Cooper et al.*, 2005; *Yamamoto-Kawai et al.*, 2008], nutrients [*Jones et al.*, 1998; *Ekwurzel et al.*, 2001; *Yamamoto-Kawai et al.*, 2008], total alkalinity [*Anderson et al.*, 2004b; *Yamamoto-Kawai et al.*, 2005; *Shadwick et al.*, 2011b], and barium concentrations [*Guay and Falkner*, 1997; *Taylor et al.*, 2003; *Guay et al.*, 2009; *Thomas et al.*, 2011]. All these tracers have limitations, an important one being the variation in these properties among Arctic rivers [*Cooper et al.*, 2008]. Nevertheless, these tracers have been used successfully to characterize pathways taken by river runoff in the Arctic Ocean and the distribution of sea ice meltwater. Available observational data remain too limited in both space and time to elucidate the mechanisms that control the seasonal distribution of freshwater tracers (e.g., TA and $\delta^{18}O$) in the Arctic Ocean, especially during the winter when sea ice forms.

[4] Because the CO_2 solubility in seawater increases with decreasing temperature, the Arctic Ocean may act as a net sink of CO_2 [*Anderson et al.*, 2004a; *Rysgaard et al.*, 2007; *Semiletov et al.*, 2007]. Part of the CO_2 taken up by the surface ocean can be transported to intermediate and greater depths as surface water density increases due to cooling and/or the addition of salt from brine drainage during sea ice formation [*Jones and Coote*, 1981; *Anderson et al.*, 1990; *Melling and Moore*, 1995; *Gibson and Trull*, 1999; *Shcherbina et al.*, 2003; *Nilsen et al.*, 2008; *Skogseth et al.*, 2008]. The southeastern Beaufort Sea, encompassing the Mackenzie Shelf, the Cape Bathurst Polynya and the Amundsen Gulf, is currently a net sink of atmospheric CO_2 (from -6.0 to -2.3 mmol CO_2 m^{-2} d^{-1} on average) during the ice-free period [*Fransson et al.*, 2009; *Mucci et al.*, 2010; *Shadwick et al.*, 2011a]. Nevertheless, the region displays strong spatial variability in seawater CO_2 fugacity (fCO_2-sw) due to sea ice coverage, freshwater input, primary production, and upwelling events. In this context, the assessment of water mass distributions and their variability is crucial to predict their response to Arctic climate change.

[5] In this study, we present the seasonal variability of TA and $\delta^{18}O$ from data collected in the southeastern Beaufort Sea during a unique, near-continuous full-year time series. The distributions of TA and $\delta^{18}O$ are then used to trace meteoric water, sea ice meltwater and other seawater masses. An optimum multiparameter (OMP) analysis is used to estimate the relative contributions of source water types to discrete parcels of seawater [*Tomczak and Large*, 1989]. Because it uses numerous tracers, OMP is a more complex and complete analysis that provides additional insights into water mass distribution, than has been used in previous studies. We investigate the seasonal variability of water mass distribution, with respect to the carbonate system parameters (1) in autumn, after the Mackenzie freshet period but before sea ice formation; (2) from winter to spring, from the onset of sea ice formation to the maximum sea ice cover (>90%); and (3) in summer, during the ice-free period.

2. Data and Methods

[6] The Canadian Arctic Shelf Exchange Study (CASES) was conducted in the southeastern Beaufort Sea, including the Mackenzie Shelf and the Cape Bathurst Polynya, between September 2003 and August 2004 (Figure 1 and Table 1). One hundred and twenty two stations were visited by the icebreaker CCGS *Amundsen* during the ice-free season, whereas the ship was ice-bound in Franklin Bay from December 2003 to the end of May 2004. Seawater samples were collected using a rosette system (24 × 12-L Niskin

Table 1. CASES Expedition Legs, Periods, Location, Number of Stations Visited, and Measured and Computed Parameters

CASES Leg	Dates	Season	Location	Number of Stations	$\delta^{18}O$	pH_t	TA	TIC	fCO_2-sw
1	30 Sep to 13 Oct 2003	autumn	Mackenzie Shelf and Cape Bathurst Polynya	13		measured	measured	measured	computed
2	19 Oct to 19 Nov 2003	autumn	Mackenzie Shelf, Beaufort Sea and Cape Bathurst Polynya	50	measured	measured	measured	measured	computed
3–6	9 Dec 2003 to 27 May 2004	winter spring	Franklin Bay	1	measured	measured	measured	measured	computed
7	4 Jun to 22 Jun 2004	spring	Cape Bathurst Poylnya	16		measured	measured	measured	computed
8	25 Jun to 1 Aug 2004	summer	Mackenzie Shelf and Cape Bathurst Polynya	37	measured	measured	measured	measured	computed
9	6 Aug to 10 Aug 2004	summer	Cape Bathurst Polynya	5		measured	measured	measured	computed

bottles) equipped with a Conductivity-Temperature-Depth sensor (CTD, Seabird® SBE 911plus) and a Seapoint® fluorometer. The temperature and conductivity probes were calibrated by the manufacturer, but a further calibration of the conductivity sensor was carried out using discrete salinity samples taken throughout the water column and analyzed on a Guildline Autosal 8400 salinometer calibrated with IAPSO standard seawater. The output of the fluorometer was calibrated against chlorophyll-*a* (Chl-*a*) concentrations measured on discrete samples taken between April and August 2004 [*Tremblay et al.*, 2008]. The CTD oxygen sensor (SBE-43) was calibrated against discrete seawater samples analyzed for dissolved oxygen concentration by Winkler titration [*Grasshoff et al.*, 1983] with a reproducibility of ± 2 μmol L^{-1}.

[7] Three parameters of the carbonate system were measured onboard in seawater samples: pH, total alkalinity (TA) and total inorganic carbon (TIC). The pH was determined colorimetrically at 25°C using a Hewlett-Packard® (HP-8453A) UV-Visible diode array spectrophotometer and a 5-cm quartz cell. Phenol red (PR) [*Robert-Baldo et al.*, 1985] and *m*-cresol purple (mCP) [*Clayton and Byrne*, 1993] were used as indicators, and measurements were carried out at the wavelengths of maximum absorbance of the protonated and deprotonated indicators (PR, 433 and 558 nm [*Byrne*, 1987]; mCP, 434 and 578 nm [*Clayton and Byrne*, 1993]). A similar procedure was carried out before and after each set of sample measurements using TRIS buffers at salinities of approximately 25 and 35 [*Millero et al.*, 1993]. All pH measurements were converted to in situ pH_t (pH reported on the total proton scale) using the in situ temperature and salinity of each sample and the HSO_4^- dissociation constants given by *Dickson* [1990]. The reproducibility and accuracy of the pH measurements, based on duplicates, were both ± 0.005 pH units or better. Total alkalinity was measured by open-cell potentiometric titration (TitraLab 865, Radiometer®) with a combined pH electrode (pHC2001, Red Rod®) and diluted HCl ($\sim$0.03 M) as a titrant. The TIC was determined by coulometric titration using a SOMMA instrument [*Johnson et al.*, 1993] fit to a UIC 5011 coulometer. Analyses of TA and TIC were conducted according to standard protocols [*Dickson and Goyet*, 1994], and the instruments were calibrated against Certified Reference Materials (CRM Batch 61, provided by A. G. Dickson, Scripps Institution of Oceanography, USA). Precisions for TA and TIC, determined from replicate samples drawn from the same Niskin bottle, varied between legs from 2 to 4 μmol kg^{-1}. The measurement of pH, TA and TIC provides an overdetermination of the carbonate system, which allows fCO_2-sw to be calculated from three possible combinations of measured parameters using the CO2SYS program [*Lewis and Wallace*, 1998] and the carbonic acid dissociation constants of *Mehrbach et al.* [1973] as refit by *Dickson and Millero* [1987]. The fCO_2-sw was computed using the combination of TA-pH or TIC-pH, because both TA and TIC were not systematically measured in all samples. The difference between the fCO_2-sw calculated from TA-pH and TIC-pH was less than 2 μatm.

[8] Oxygen isotopes were analyzed by the CO_2 equilibration method [*Epstein and Mayeda*, 1953] on a DeltaPlus XP mass spectrometer (Thermo Finnigan) at the University of Ottawa (G.G. Hatch Isotope Laboratory). The oxygen isotope composition of water is reported on the $\delta^{18}O$ notation, defined as the $^{18}O/^{16}O$ ratio of a sample relative to the Vienna Standard Mean Ocean Water (V-SMOW) according to: $\delta^{18}O = (({}^{18}O/{}^{16}O)_{sample}/({}^{18}O/{}^{16}O)_{V\text{-}SMOW} - 1) \times 10^3$[‰]. The $\delta^{18}O$ was measured on water samples collected during CASES legs 2, 8 and throughout the overwinter period, legs 3–6 (Table 1). The $\delta^{18}O$ of seawater was measured to a precision of ± 0.05‰, based on the analysis of random duplicate samples.

2.1. Regional Water Mass Analysis

[9] The annual mean freshwater input to the Arctic Ocean is dominated by river discharge (38%), inflow of relatively low-salinity Pacific Water through the Bering Strait (30%) and net precipitation (24%) [*Serreze et al.*, 2006]. With a mean annual discharge of about 330 km^3 yr^{-1}, the Mackenzie River is the main source of river water to the southeastern Beaufort Sea. The Mackenzie River flow is seasonally variable and the peak discharge (approximately 30 000 m^3 s^{-1}) typically occurs at the end of May [*Carmack and Macdonald*, 2002]. Sea ice meltwater is another significant source of freshwater to the Arctic Ocean. The Arctic sea ice grows through the winter, reaching its largest extent in March, after which time it shrinks through the spring and summer, reaching its smallest extent in September [*Arrigo and van Dijken*, 2004; *Barber and Hanesiak*, 2004].

[10] According to previous studies [*Carmack et al.*, 1989; *Macdonald et al.*, 1989, 2002], six main source-water types (end-member water masses) can be recognized

Table 2. Source-Water Types and Their Characteristic Properties Used in the OMP Analysis[a]

Water Types	Temperature (°C)	Salinity (psu)	O_2 (μmol L^{-1})	$\delta^{18}O$ (‰)	TA (μmol kg^{-1})	TIC (μmol kg^{-1})	pH_t	fCO_2-sw (μatm)
Mackenzie water (MW)	0 to +16	0	330 ± 20	−18.9 ± 0.1[b]	1618 ± 55[b]	1700 ± 60	8.43 ± 0.07[c]	>500[d]
Sea ice melt (SIM)	0 ± 0.2	4.7 ± 0.5[e,f]	380 ± 15	−2.0 ± 0.5[g,h]	415 ± 35[e,f]	330 ± 30[e,f]	>8.0	280 ± 30
Polar mixed layer (winter) (PML)	−1.65 ± 0.05	32 ± 0.1[i]	340 ± 18	−2.5 ± 0.2[i]	2256 ± 12	2162 ± 14	8.05 ± 0.04	415 ± 23
Upper halocline water (UHW)	−1.44 ± 0.04	33.1 ± 0.1[j]	270 ± 10	−1.6 ± 0.1	2283 ± 8	2228 ± 8	7.88 ± 0.03	580 ± 29
Atlantic water (ATW)	+0.48 ± 0.05	34.82 ± 0.02	260 ± 12	+0.27 ± 0.05	2297 ± 6	2168 ± 14	8.06 ± 0.03	356 ± 28
Canada Basin deep water (CBDW)	−0.4 ± 0.05[k]	34.95 ± 0.02[k]	300 ± 10	+0.35 ± 0.05[l]	2300 ± 4	2153 ± 5	8.08 ± 0.02	311 ± 12

[a]The values used for the source water types are derived from both our data set and the literature. See the following footnotes.
[b]*Cooper et al.* [2008].
[c]*Retamal et al.* [2008].
[d]*Vallières et al.* [2008].
[e]*Rysgaard et al.* [2007].
[f]*Miller et al.* [2011].
[g]*Eicken et al.* [2002].
[h]*Yamamoto-Kawai et al.* [2009].
[i]*Macdonald et al.* [1995].
[j]*Macdonald et al.* [1989].
[k]*Carmack et al.* [1989].
[l]*Ekwurzel et al.* [2001].

in the southeastern Beaufort Sea (Table 2): (1) meteoric water (MW, Mackenzie River plus precipitation), (2) sea ice melt (SIM), (3) polar mixed layer (PML), (4) upper halocline water (UHW, modified Pacific Water with core salinity of 33.1 psu), (5) Atlantic Water (ATW), and (6) the Canada Basin deep water (CBDW). In this study, the PML is the considered to be the surface water that becomes mixed to uniform, or almost uniform, properties during winter. This layer of water has its properties altered by the addition of SIM and MW in summer, and by the removal of SIM through ice formation in winter. Because the properties of the PML vary depending on the strength of sea ice formation in a given winter and the amounts of SIM or MW supplied in summer, the PML cannot be defined precisely except in the context of a particular location and year. Here, we take advantage of the CASES project design, which provided samples over a full-year cycle, and use the winter profile data to define depth and properties of the PML. Most prior studies inferred such properties from summer profiles. Accordingly, we defined the winter PML as the water mass located just below the surface mixed layer (SML) in summer whose highest salinity (32) is observed during the winter. Thus, the effect of brine rejection generated by ice formation is included in our definition of the winter PML. The SML is defined as the upper layer of the ocean with quasi-homogeneous potential density above the main pycnocline. Vertical profiles of potential density were used to calculate the depth of the base of the SML (usually 30 m), and defined as the depth at which the density increases by 20% of the mean density of the upper 10 m [e.g., *Shaw et al.*, 2009].

[11] In the Canada Basin, a strong vertical density gradient separates nutrient-poor surface waters (i.e., the PML) from the underlying nutrient-rich upper halocline water [*Aagaard et al.*, 1981; *Jones and Anderson*, 1986; *Rudels et al.*, 2004]. The UHW is mainly fed by Pacific Water flowing in through Bering Strait, undergoing transformation as it crosses the Chukchi Sea shelf and entering the Canada Basin through the Barrow and Herald Canyons [*Pickart*, 2004; *Woodgate et al.*, 2006]. The UHW is typically found between 120 and 180 m depth and is recognizable as intermediate salinity water (33.1) with a temperature minimum (−1.5°C) and relatively low oxygen concentrations (270 μmol L^{-1}) [*Jones et al.*, 1998; *McLaughlin et al.*, 2004; *Shimada et al.*, 2006]. This temperature minimum is supported, in part, by intermittent contributions of dense water produced by ice formation on adjacent shelves [*Melling and Moore*, 1995; *Mathis et al.*, 2007]. The UHW is also recognizable by its high nutrient [*Jones et al.*, 2003; *Yamamoto-Kawai et al.*, 2008] and TIC concentrations [*Shadwick et al.*, 2009; *Mucci et al.*, 2010], as it flows from the Arctic Ocean to the North Atlantic via the Canadian Arctic Archipelago and Fram Strait [*Rudels et al.*, 2004; *Jones et al.*, 2008]. In this paper, the Pacific Water inflow through the Bering Strait is not considered as a source of freshwater [e.g., *Serreze et al.*, 2006] but as a distinct saline end-member [*Macdonald et al.*, 2002], even though its salinity (33.1) is lower than the deep Arctic Ocean (34.82). Atlantic water is mainly formed by water entering the Canada Basin from the Makarov Basin via Fram Strait and the Barents Sea [*McLaughlin et al.*, 1996; *Rudels et al.*, 2004]. ATW is present below the deep halocline, at depths of about 200 m, and it is characterized by a salinity of 34.82, a deep temperature maximum (+0.5°C), a minimum oxygen and relatively low nutrient and TIC concentrations [*Jones and Anderson*, 1986; *Macdonald et al.*, 1989; *McLaughlin et al.*, 2004].

2.2. Use of Multiple Water Mass Tracers and Water Mass Calculations

[12] The application of salinity (S), TA and $\delta^{18}O$ to distinguish the two major sources of freshwater, meteoric water and sea ice melt, to seawater is well established [*Östlund and Hut*, 1984; *Macdonald et al.*, 1989; *Ekwurzel et al.*, 2001; *Anderson et al.*, 2004b; *Bauch et al.*, 2005; *Yamamoto-Kawai et al.*, 2005; *Jones et al.*, 2008]. Provided chemical properties of the end-members are well defined and appropriate to the study region in the Beaufort Sea [*Macdonald et al.*, 1995], the relative contributions of meteoric water (F_{MW}), sea ice melt (F_{SIM}), upper halocline water (F_{UHW}) and Atlantic water

Table 3. Weights Applied to Each Parameter Used in the OMP Analysis

Parameters	Precision	Weights Used in OMP Analysis: Above the UHW (Salinity < 33.1)	Weights Used in OMP Analysis: Below the UHW (Salinity > 33.1)
Temperature (°C)	0.01	1	25
Salinity (psu)	0.01	25	25
Dissolved O_2 (μmol L^{-1})	2.0	1	5
Total alkalinity (μmol kg^{-1})	2.0	25	1
$\delta^{18}O$ (‰)	0.05	25	5
Mass conservation		25	25

(F_{ATW}) in a given parcel of water can be computed using the following mass balance equations for salt, TA and $d^{18}O$:

$$F_{MW} + F_{SIM} + F_{UHW} + F_{ATW} = 1, \quad (1)$$

$$F_{MW}S_{MW} + F_{SIM}S_{SIM} + F_{UHW}S_{UHW} + F_{ATW}S_{ATW} = S, \quad (2)$$

$$F_{MW}TA_{MW} + F_{SIM}TA_{SIM} + F_{UHW}TA_{UHW} + F_{ATW}TA_{ATW} = TA, \quad (3)$$

$$F_{MW}\delta^{18}O_{MW} + F_{SIM}\delta^{18}O_{SIM} + F_{UHW}\delta^{18}O_{UHW} + F_{ATW}\delta^{18}O_{ATW} = \delta^{18}O. \quad (4)$$

[13] This method is widely used but typically with only two tracers, salinity-$\delta^{18}O$ [e.g., *Östlund and Hut*, 1984] or salinity-TA [*Anderson et al.*, 2004b; *Jones et al.*, 2008], i.e., in three-component mixing models. To our knowledge, the combination of salinity-$\delta^{18}O$ and salinity-TA has been used only by *Yamamoto-Kawai et al.* [2005] to investigate freshwater and brine distributions in the Arctic Ocean. However, results from previous studies should be interpreted with caution because the calculated water mass compositions are sensitive to the assigned properties of each end-member.

[14] There are at least three main issues to consider in assigning end-members for this kind of tracer analysis:

[15] 1. Inputs of TA and $\delta^{18}O$ by MW and SIM are variable in both time and space. Hence, the end-member properties (S, TA and $\delta^{18}O$) and the computed fractions are site dependent.

[16] 2. As sea ice forms, brine release increases the salinity and TA of the surface mixed layer but decreases the $\delta^{18}O$, since ^{18}O is preferentially incorporated in the freezing ice [*Lehmann and Siegenthaler*, 1991]. In the system of equations defined above ((1)–(4)), brine rejected from ice into the water results in a "negative" sea ice melt fraction that reflects sea ice growth and adds negative buoyancy to the SML. Changes in salinity, TA and $\delta^{18}O$ are most noticeable in the SML, whose maximum thickness at our study site was 50 m in late winter, even if mixing with deeper waters does occur but typically limited to the upper 100 m. The effects of sea ice formation and brine rejection on the SML properties are not completely understood, and the rate of brine rejection varies with ice thickness and growth rate in a manner that has not been well quantified. A detailed study of the chemical evolution of the SML during ice formation in this region during two non-consecutive years and the processes at play are the subject of an upcoming paper.

[17] 3. The definition of the seawater end-member in the Arctic Ocean differs from one study to another for the very practical reason that n number of tracers permits solutions for only n+1 water masses, which with two tracers implies that one and only one saline end-member may be used. Depending on the study objectives and location, the saline end-member has been assigned to the UHW or Pacific Water [*Macdonald et al.*, 1989, 1995, 2002; *Yamamoto-Kawai et al.*, 2009], Atlantic Water [*Östlund and Hut*, 1984; *Schlosser et al.*, 2002; *Anderson et al.*, 2004b; *Yamamoto-Kawai et al.*, 2005; *Newton et al.*, 2008], and the Polar Mixed Layer [*Alkire and Trefry*, 2006]. Since the computation of freshwater and sea ice melt fractions (and inventory) depend on the seawater end-member definition, absolute results cannot be compared directly among studies using different saline end-member baselines, although patterns in distributions may be compared.

2.3. OMP Analysis

[18] In this study, we used an optimum multiparameter (OMP) algorithm to quantify the relative contributions of the different source water types to the observed data. The OMP analysis [*Karstensen*, 2006] is a weighted, nonnegative, linear least squares, mass balance algorithm developed from the earlier work of *Mackas et al.* [1987] and *Tomczak and Large* [1989]. This algorithm has been extensively used to determine water mass distribution in many areas of the world ocean [*Leffanue and Tomczak*, 2004, and references therein] including the Greenland Sea [*Karstensen et al.*, 2005; *Jeansson et al.*, 2008], the Canadian Beaufort Sea [*Macdonald et al.*, 1989] and the Alaskan Beaufort Sea [*Alkire and Trefry*, 2006]. Briefly, the method finds the best fitting fraction (x) of (n+1) source water types that contribute to the (n) observed values of the selected tracers in a parcel of water via solution of an over-determined system of linear equations that minimizes the residual error. Boundary conditions were applied to the method to guarantee that all fractions calculated were positive and that the sum of all fractions was 100% (mass conservation).

[19] The OMP analysis was initially used to distinguish and calculate the relative contributions of different water masses in a parcel of water using temperature and salinity as conservative tracers, as well as nutrient data [*Mackas et al.*, 1987]. In this study, we used salinity, TA, and $\delta^{18}O$ as conservative tracers as well as temperature and O_2 concentration as non-conservative tracers, to constrain the water mass analysis. Non-conservative tracers should be applied with caution in OMP, because of seasonal variations in the SML. For example, the temperature of the Mackenzie water ranges from 0°C in winter to +16°C in summer while the temperature of the SML ranges from −1.7°C to +7°C. Dissolved O_2 concentration was also used as a non-conservative tracer, because it is a function of temperature (e.g., O_2 solubility increases with decreasing temperature and salinity), primary production, and biological respiration. Consequently, a relatively low weight was assigned to temperature and O_2 data above the UHW for the OMP analysis (Table 3). Salinity, TA and $\delta^{18}O$ data were used with a relatively heavy weight to distinguish MW and SIM from the PML. Conversely, the

weight assigned to the temperature and O_2 were increased below the UHW, where these tracers approach conservative behavior, to discriminate between the cold UHW and the relatively warm ATW and CBDW. The characteristic properties of the end-members are variable in both time and space, but we refer to our data set and previous studies to define the most representative properties for each source water type (Table 2). The end-member matrix and sample observations were multiplied by a diagonal weight matrix to account for differences in tracer reliability, environmental variability, and precision of the data (Table 3). The OMP method has the advantage that the solution is "spread" over more tracers and is therefore not as sensitive to error in individual tracers. The error associated with the water mass fraction analysis was estimated to be about ± 10% of the fractional values, which was similar to that estimated by *Macdonald et al.* [1989].

3. Results

[20] A total of 1346 measurements of TA, TIC and pH_t and 485 measurements of $\delta^{18}O$ were acquired during the 11-month field study. Vertical distributions of temperature, salinity, dissolved O_2 concentration, $\delta^{18}O$, TA, TIC, pH_t and computed fCO_2-sw, throughout the study area and the sampling period, are shown in Figure 2. Vertical distributions vary seasonally for all parameters in the SML, largely due to MW inputs and to sea ice freezing and melting processes. Conversely, weak seasonal variability was observed below the UHW (~150 m depth), and seawater properties were less variable. Sea surface temperatures ranged from −1.7°C in winter to +16°C in summer, with the highest temperature observed at the mouth of the Mackenzie River. Sea surface salinities ranged from nearly 0 in the Mackenzie River delta to 32.1 in the vicinity of Cape Bathurst.

[21] The highest O_2 concentrations (440 μmol L^{-1}, 120% O_2 saturation) were recorded between June and August 2004 in surface water on the eastern part of the Mackenzie Shelf and in the Cape Bathurst Polynya. These peaks of O_2 were frequently associated with relatively high Chl-*a* concentrations (>3 μg L^{-1}) and, thus, had been generated by primary production. Below the SML, oxygen concentrations decreased with depth as a result of organic matter degradation by bacterial respiration, as well as mixing with the O_2-depleted UHW. The O_2 minimum zone (O_2 < 250 μmol L^{-1}, <70% O_2 saturation) was located around 200 ± 60 m depth, along the deep pycnocline. At greater depth, the O_2 concentrations increase to 300 μmol L^{-1} (>80% O_2 saturation) in the Canada Basin deep water.

[22] In the Beaufort Sea, the $\delta^{18}O$ of seawater varies as a function of freshwater inputs by river runoff (−19‰), and sea ice melt (−2.0‰) as well as mixing with deep water (+0.35‰). Accordingly, we observed the lowest $\delta^{18}O$ values (−6.0‰) in the low-salinity surface water of the Mackenzie Shelf while the highest (+0.3‰) were observed below 300 m depth in the Canada Basin.

[23] Total alkalinity increases with salinity and therefore, with depth, ranging from 1310 μmol kg^{-1} at the surface to 2320 μmol kg^{-1} at the bottom. Similarly, TIC concentrations ranged from 1280 μmol kg^{-1} in surface water to 2155 μmol kg^{-1} at the bottom. There was a positive correlation between TA and TIC (TA = 266.7+0.92 × TIC; r^2 = 0.94; n = 1317), but TIC concentrations reach maximum values (>2220 μmol kg^{-1}) at 140 ± 30 m depth, while alkalinity increased monotonically with depth. The additional TIC observed at this depth may have been acquired in situ (metabolic CO_2 generated through organic matter mineralization) or imported with Pacific water. The sea surface pH_t in the southeastern Beaufort Sea was usually close to 8.10 ± 0.05 throughout our sampling period. The pH of relatively low-salinity surface water found in the Mackenzie River delta could range from 7.8 in winter (low river discharge) to 8.5 in summer (high river discharge) [*Millot et al.*, 2003; *Retamal et al.*, 2008]. In our data set, the pH_t of seawater reached a minimum value of 7.87 ± 0.02 at 140 ± 30 m depth, corresponding to the TIC maximum. In the SML, fCO_2-sw was mostly undersaturated (328 ± 55 μatm) with respect to the atmosphere (fCO_2-atm = 380 ± 5 μatm, recorded at Point Barrow, Alaska [*Keeling et al.*, 2008]). The maximum fCO_2-sw zone (>550 μatm) was located around 140 ± 30 m depth, corresponding to the UHW.

3.1. Seasonal Variability of Conservative Tracers (Salinity, TA, and $\delta^{18}O$)

[24] Based on the seasonality of the Mackenzie River flow and ice cover during the CASES expedition (Figure 3), we sub-divided our data set into three main sampling periods: (1) autumn 2003, well past the Mackenzie River freshet but before sea ice formation; (2) winter-spring 2003–2004, during the sea ice covered period; and (3) summer 2004, the ice-free period. The seasonality of the SML properties is highlighted by T-S-fCO_2-sw diagrams for the three study periods defined above (Figure 4). In autumn 2003 (Figure 4a), the SML (exhibiting sea surface salinities < 30) was a mix of MW, SIM and summer SML with relatively high subsurface temperatures (up to 0.8°C). The average fCO_2-sw was 292 ± 27 μatm, and therefore, the SML was undersaturated with respect to the average atmospheric fCO_2 value (380 ± 5 μatm). During the winter, cooling and sea ice formation changed the SML properties. The T-S data fall along the freezing line, and the newly formed winter PML clearly stands out (Figure 4b). Over the winter, the average fCO_2-sw increased to 370 ± 33 μatm in the mixed layer as a result of brine rejection, bacterial respiration [*Sherr and Sherr*, 2003] and possibly air-sea CO_2 exchange in the Cape Bathurst Polynya [*Else et al.*, 2011]. In summer (Figure 4c), freshwater input from MW and SIM generated a strong pycnocline in the surface waters. In response to freshwater inputs, the salinity of the SML decreased to below 29, while long daylight hours together with the loss of ice cover produced sea surface temperatures up to +7°C in the Cape Bathurst Polynya. Very low-salinity surface water (<10) with high fCO_2-sw (>500 μatm) was observed at the Mackenzie River mouth (indicated by 'MW' in Figure 4c). Conversely, relatively low sea surface salinities (<30) with very low fCO_2-sw (<300 μatm) were observed beyond the shelf break and close to the ice pack. Deeper (Figure 4d), fCO_2-sw values were highest in the UHW (greater than 600 μatm) throughout the year, whereas the ATW and CBDW had lower fCO_2-sw values (less than 360 μatm), close to equilibrium with the atmosphere.

[25] In order to define the best characteristic properties of the end-member water masses, we now examine the seasonal co-variations of salinity, TA and $\delta^{18}O$ (Figure 5). The relationships between salinity, TA and $\delta^{18}O$ show the data to be

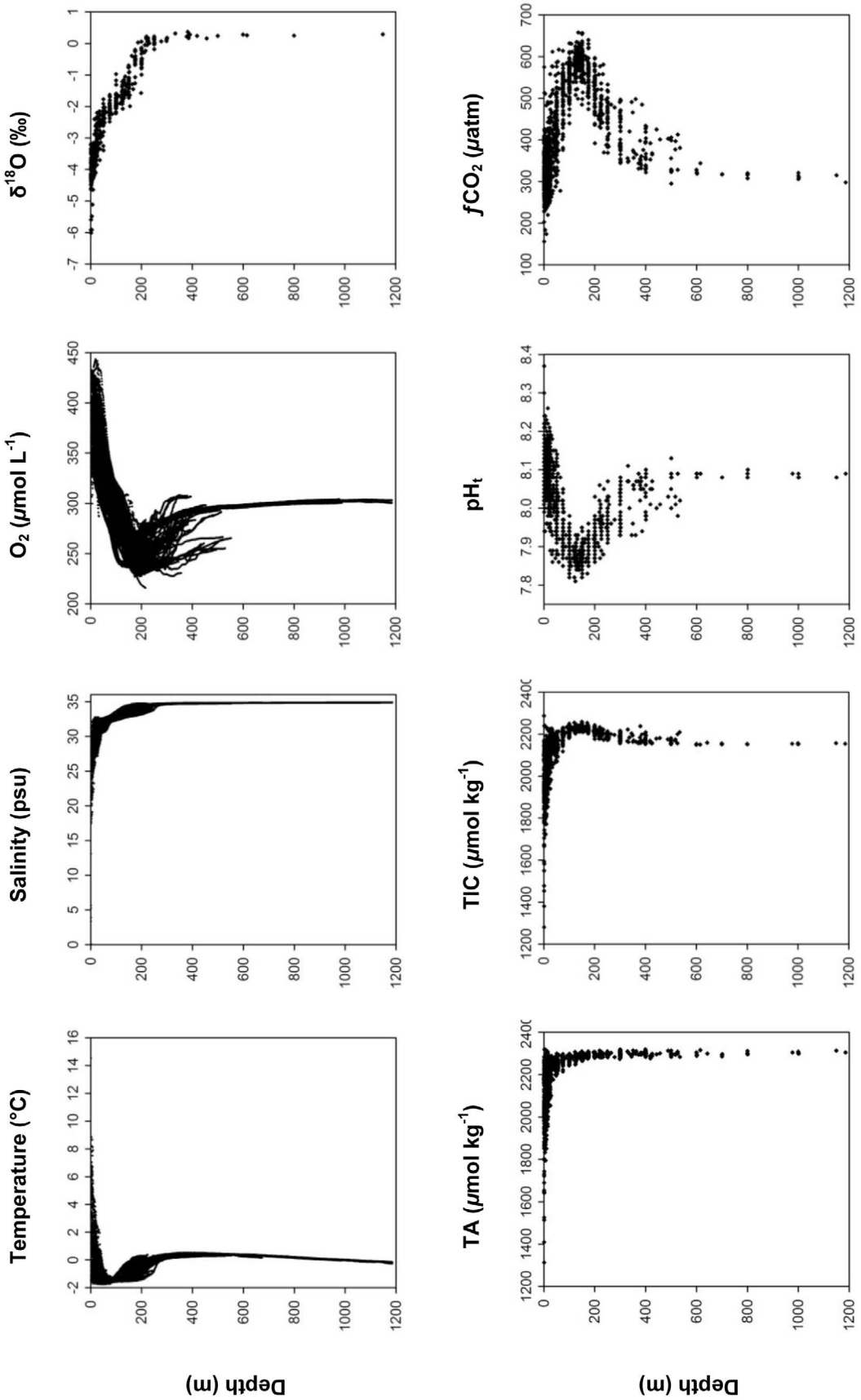

Figure 2. Vertical distribution of temperature (°C), salinity (psu), dissolved O_2 concentration (μmol L^{-1}), $\delta^{18}O$ (‰), total alkalinity (μmol kg^{-1}), total inorganic carbon (μmol kg^{-1}), pH_t and fCO_2-sw (μatm) from September 2003 to August 2004.

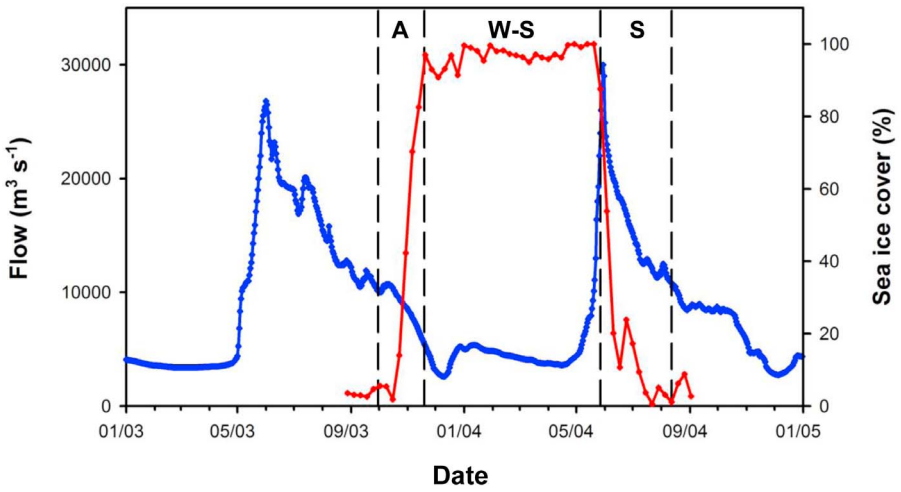

Figure 3. Mackenzie River flow (blue line) and sea ice cover in Franklin Bay (red line) during the CASES expedition. The Mackenzie River discharge was recorded at Tsiigehtchic by Water Survey Environment Canada. The dashed lines indicate the three seasons examined in this study (A, autumn; W-S, winter-spring; S, summer).

organized by two mixing lines, one reflecting SIM as the freshwater end-member and the other, MW. These two mixing lines converge in the winter PML (S = 32). In autumn (Figure 5a), surface waters with relatively low salinity (less than 25) had relatively low TA (<1900 μmol kg^{-1}) and δ^{18}O (<−4‰) compared to the deeper, more saline waters (S > 32). During the winter (Figure 5b), the salinity of the SML increased from 28 to 31.5 and, concomitantly, TA and δ^{18}O increased to 2260 μmol kg^{-1} and −2.5‰, respectively. The properties of the SML (salinity, TA and δ^{18}O) converge gradually to those of the winter PML. Hence, the contribution of freshwater to the mixed layer decreased from summer to winter due to a decline in MW input, the withdrawal of SIM into the growing ice cover, and probably the loss of freshwater components by exchange with the interior ocean [*Macdonald et al.*, 1989]. In summer (Figure 5c), the TA and δ^{18}O distributions again showed evidence of freshwater inputs to the surface waters from both MW and SIM, but with much greater variability than in autumn. At low salinities (less than 25), the data points from the Mackenzie Shelf tended toward the MW-PML mixing lines, whereas those from the Beaufort Sea and Cape Bathurst Polynya tended toward the SIM-PLM mixing line.

[26] The combination of S-TA-δ^{18}O, when these data are available, is a powerful tool to resolve the freshwater cycle in the Arctic Ocean than either tracer alone. Plots of TA versus δ^{18}O (Figures 5a, bottom–5c, bottom) provide a simple way to distinguish between MW and SIM components. In the autumn of 2003, data points from the mixed layer plotted nearly midway between the MW-PML and SIM-PML mixing lines, implying equivalent and well-mixed contributions from MW and SIM. In the winter of 2003–2004, the contribution of SIM was very low and the relatively low salinity observed in the mixed layer (S < 32) was attributed to a small fraction of residual MW. In the summer of 2004, the samples collected on the Mackenzie Shelf had relatively low δ^{18}O (−6‰) and TA (2100 μmol kg^{-1}) and nearly follow the MW-PML line, implying that mixing with the Mackenzie plume dominates in this region. In contrast, samples collected beyond the shelf break and in the Cape Bathurst Polynya plot along the SIM-PML line.

3.2. A Winter Time Series in Franklin Bay

[27] Few experimental studies have investigated the effect of sea ice formation and brine production on under-ice water properties [e.g., *Pipko et al.*, 2002; *Papadimitriou et al.*, 2004; *Nomura et al.*, 2006; *Delille et al.*, 2007; *Rysgaard et al.*, 2007; *Miller et al.*, 2011], and it consequently remains poorly constrained. The CASES data set provide an opportunity to evaluate changes in the SML properties during landfast sea ice formation and brine rejection based on a unique time series of 33 vertical profiles recorded over the winter and spring of 2003–2004 in Franklin Bay (Figure 6). Here, we examined only the direct impacts of sea ice processes on the SML properties, while the effects on the carbonate parameters are discussed in detail by *Miller et al.* [2011].

[28] During the winter, stratification was mostly defined by a salinity gradient and the presence of a relatively stable SML whose thickness (0–30 m depth) varied with the tidal cycle [*Gratton et al.*, 2006]. The seawater temperature was close to the freezing point (−1.5 ± 0.2°C) down to 150 m depth and increased to 0°C near the bottom. In the SML, salinity increased from 28 to 31.5 between December 2003 and March 2004, consistent with brine rejection from sea ice formation and vertical mixing. Chlorophyll-*a* concentrations were low throughout most of the time series, with values less than 0.2 μg L^{-1} in the SML after the autumn bloom, decreasing until mid-January 2004 and remaining extremely low (<0.05 μg L^{-1}) until March. There was a slow and progressive increase of Chl-*a* to 0.3 μg L^{-1} in May, prior to the onset of ice melt and the June 2004 spring bloom when Chl-*a* concentrations exceeded 2 μg L^{-1} [*Tremblay et al.*, 2008]. Chl-*a* data show that primary production was extremely low during most of the winter time series, implying that CO_2 biological uptake by the planktonic community was negligible.

[29] During the winter, TA increased in the SML, from 2120 to 2260 μmol kg^{-1}, while it was nearly constant (2295 ± 6 μmol kg^{-1}) below 150 m depth. Similarly, TIC

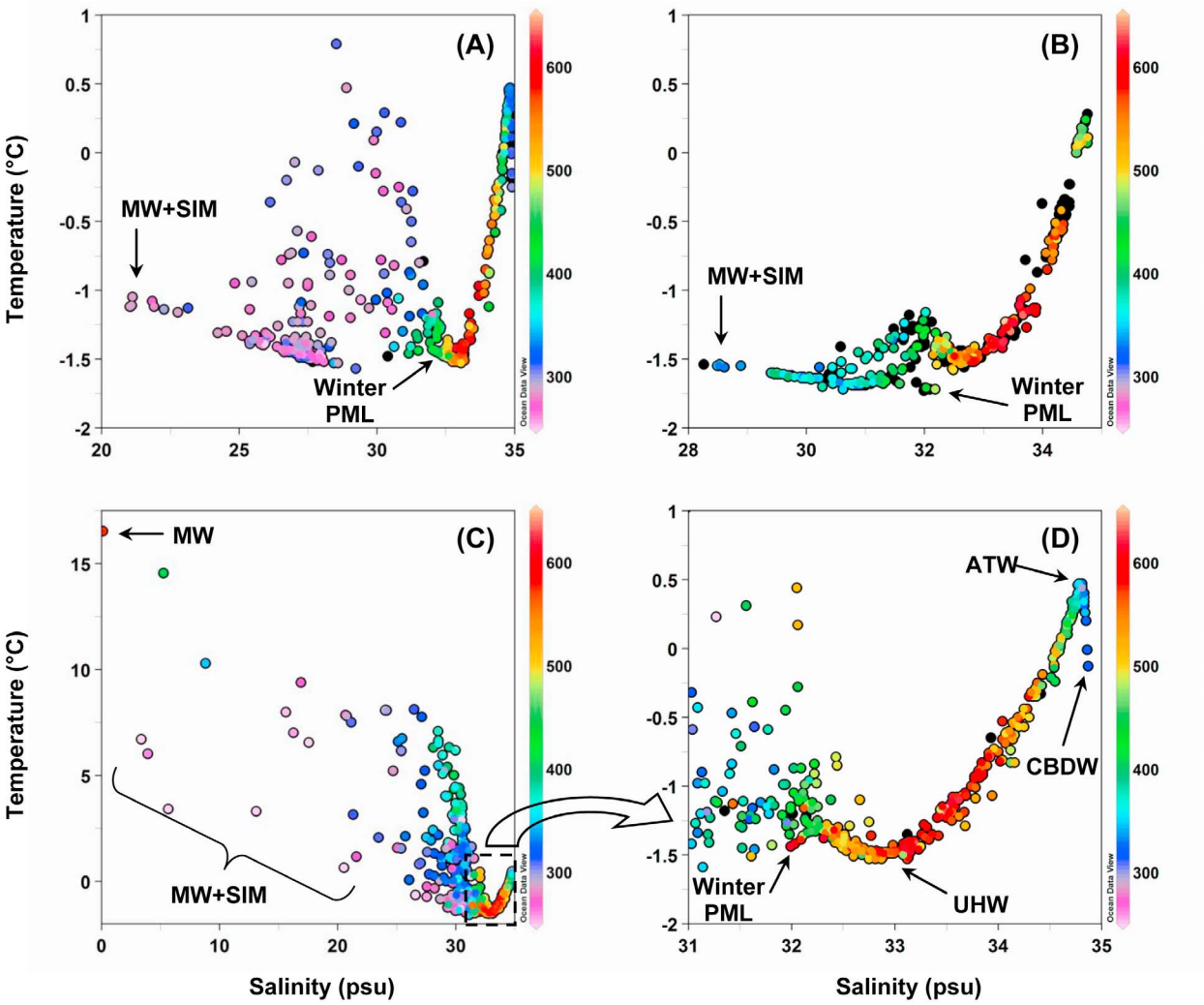

Figure 4. T-S diagrams with fCO_2-sw (μatm) for (a) the autumn 2003, (b) the winter-spring 2003–2004, and the summer 2004 (c) for the full salinity range and (d) for an expanded salinity scale. Note that the temperature and salinity scales change between seasons. Black dots indicate that no fCO_2-sw data was computed for these samples. The source water types are defined as follow: Mackenzie water (MW), sea ice melt (SIM), winter polar mixed layer (PML), upper halocline water (UHW), Atlantic water (ATW), and Canada Basin deep water (CBDW).

concentrations increased from 2080 to 2160 μmol kg^{-1} in the SML, whereas the highest concentrations (>2230 μmol kg^{-1}) were always recorded around 150 m depth. The vertical pH_t distribution shows the same pattern, with pH_t ranging from 8.05 to 8.12 in the SML, and the lowest pH_t values found around 150 m depth. The average fCO_2-sw in the SML increased slightly from 350 $\pm$ 20 μatm in early December 2003 to 376 $\pm$ 27 μatm in late April 2004. Hence, the SML was slightly undersaturated with respect to atmospheric CO_2 (380 $\pm$ 5 μatm) in early December 2003 and approached saturation by late April 2004. The average fCO_2-sw then fell to 335 $\pm$ 55 μatm in May 2004, concomitant with an increase in Chl-*a* concentration, and probably due to ice algae production. The highest fCO_2-sw values (>600 μatm) were found in the UHL, around 150 m depth. The $\delta^{18}O$ increased from -4.1 to -2.6‰ in the SML but remained nearly invariant (-0.10 ± 0.25‰) below 150 m depth. The increase of $\delta^{18}O$ in the SML cannot be explained by the formation of sea ice, since ^{18}O is preferentially incorporated in the freezing ice [*Lehmann and Siegenthaler*, 1991]. Therefore, sea ice formation would lead to a decrease in $\delta^{18}O$ in the SML as the ice formed, rather than an increase. The trend of $\delta^{18}O$ in the mixed layer indicates that the seawater fraction at our study site increased due to either vertical mixing or advection from offshore, as runoff declined to the annual minimum at the end of the winter.

[30] On 22 December 2003, relatively high temperature (-1.3°C), salinity (32), TA (2248 μmol kg^{-1}), TIC (2168 μmol kg^{-1}) and $\delta^{18}O$ (-2.4‰) were observed at 20 m depth. The properties of the upwelled water were very close to those of the winter PML. These anomalies were also observed between 100 and 200 m depth with a clear rise of the halocline level. Such perturbations of the water column stratification were assigned to the passage of a

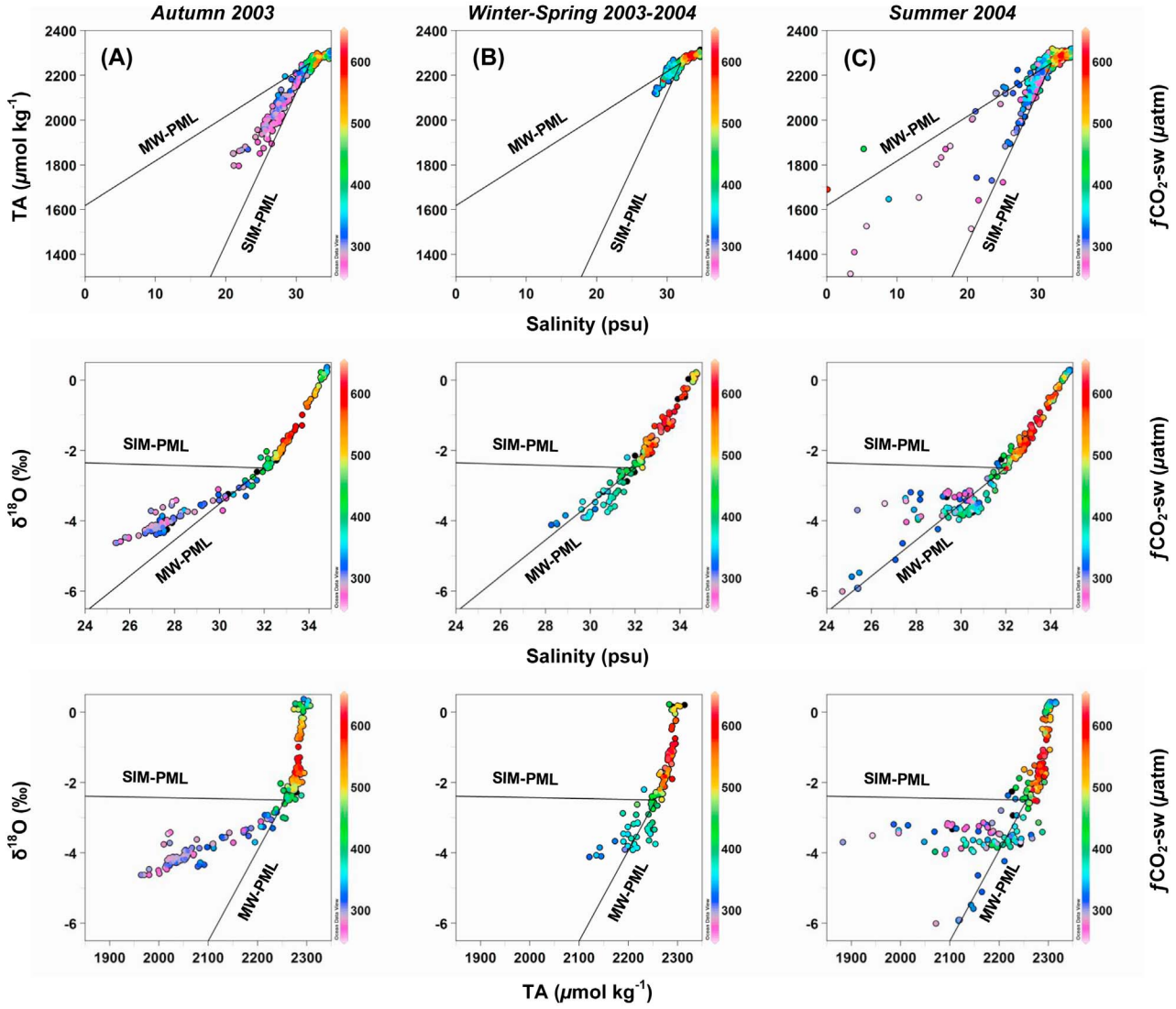

Figure 5. Seasonal variability of total alkalinity (μmol kg^{-1}) versus salinity, δ^{18}O (‰) versus salinity, and δ^{18}O versus total alkalinity with fCO_2-sw (μatm). Black dots indicate that no fCO_2-sw data was computed for these samples. The two straight lines represent the mixing lines of the winter polar mixed layer (PML) with Mackenzie water (MW) and sea ice melt (SIM), respectively. The water mass properties are defined in Table 2.

deep anticyclonic eddy through the winter station [*Tremblay et al.*, 2008].

4. Discussion

4.1. Definition of Source Water Types

[31] Referring to previous studies and our own data set, we now define the most representative properties for each source water types that are appropriate for our water mass analysis in the southeastern Beaufort Sea (Table 2). The total alkalinity of the Mackenzie River is relatively high (greater than 1500 μmol kg^{-1}) as a result of organic matter degradation and limestone weathering within its drainage basin [*Telang et al.*, 1991]. *Millot et al.* [2003] reported TA ranging from 2080 to 2380 μmol kg^{-1} for August 1996, when the Mackenzie River discharge was 16,200 m^3 s^{-1}. More recently, *Cooper et al.* [2008] reported on the seasonal variability of the Mackenzie River discharge from 2003 to 2006, when TA ranged from 1200 to 1600 μmol kg^{-1} in summer and from 1600 to 2000 μmol kg^{-1} in autumn and winter, with an annual average TA of 1618 $\pm$ 55 μmol kg^{-1}. Those water samples were collected at Tsiigehtchic (Arctic Red River), located more than 200 km upstream from the Mackenzie River delta, and one could expect a higher TA value at the Mackenzie River mouth. In our data set, one sample collected at the Mackenzie River mouth in summer 2004 had salinity close to zero and a TA of 1690 μmol kg^{-1}. However, we used the annual average TA of 1618 $\pm$ 55 μmol kg^{-1} to characterize the Mackenzie River input [*Cooper et al.*, 2008].

[32] In this study, the δ^{18}O data set does not cover the entire salinity range (0–35). Hence, we refer to previous studies on the Mackenzie Shelf [*Macdonald et al.*, 1989, 1999b] and in the Mackenzie River [*Krouse and Mackay*,

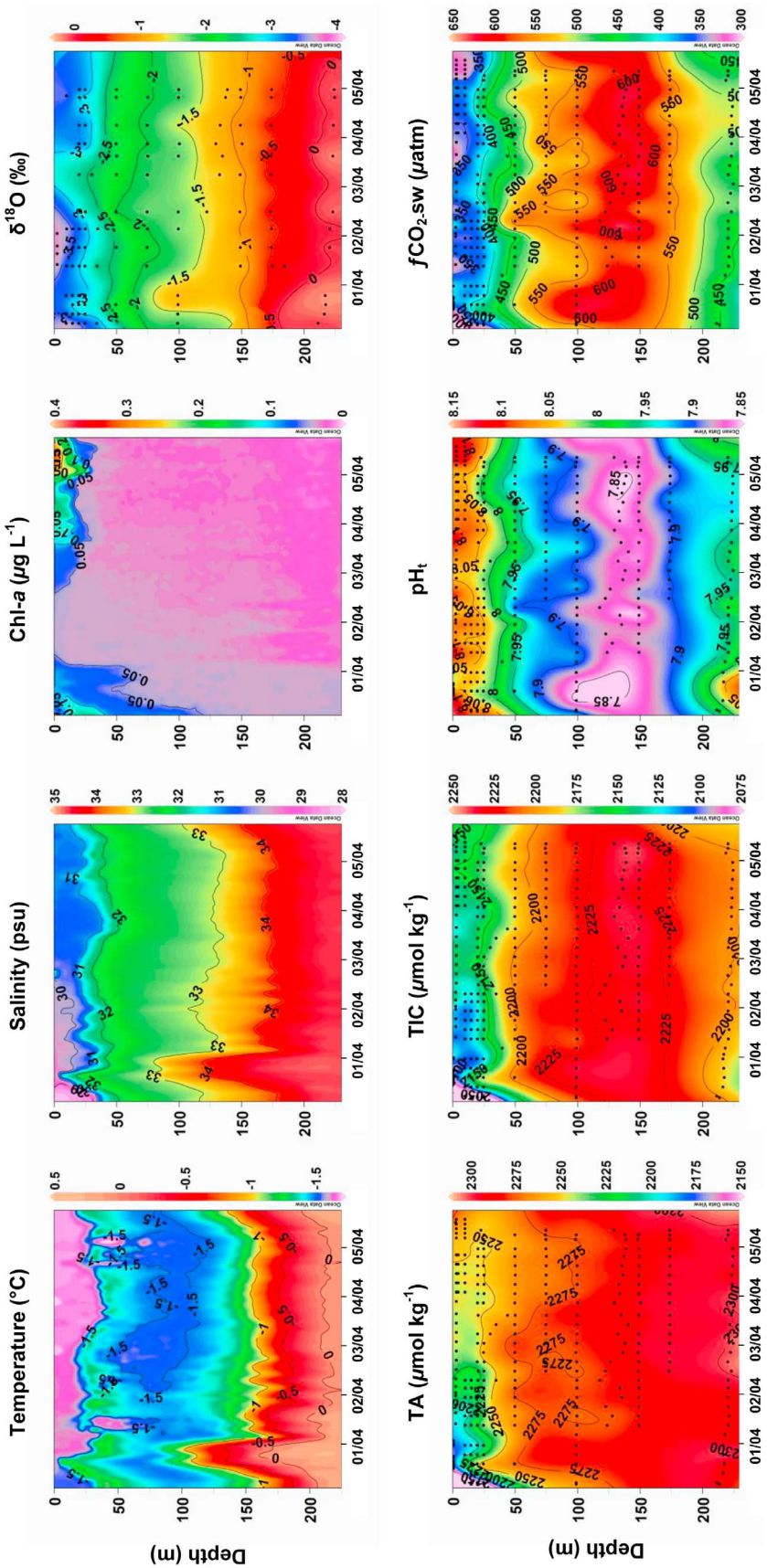

Figure 6. Time series of the vertical distribution of temperature (°C), salinity (psu), chlorophyll-*a* (μg L^{-1}), δ^{18}O (‰), total alkalinity (μmol kg^{-1}), total inorganic carbon (μmol kg^{-1}), pH_t and fCO_2-sw (μatm) from December 2003 to May 2004 at the CASES winter station located in Franklin Bay. The CTD sampling frequency was once a day whereas other parameters were measured once a week.

1971; *Cooper et al.*, 2008; *Yi et al.*, 2010] to understand variations in $\delta^{18}O$ at lower salinities (less than 25). The $\delta^{18}O$ of the Mackenzie River water ranges from −20.5 to −18.2‰, depending on water origin and river flow [*Cooper et al.*, 2008]. During very high flow in May and June, the $\delta^{18}O$ signature of the Mackenzie River water reaches an annual minimum of −20.5‰ [*Yi et al.*, 2010]. As the TA and $\delta^{18}O$ signatures for the Mackenzie River vary with flow, it is difficult to assign set values for these two geochemical tracers. Nevertheless, we set the $\delta^{18}O$ signature for the Mackenzie River at -18.9 ± 0.1‰, which is the annual average reported by *Cooper et al.* [2008].

[33] The salinity, TA and $\delta^{18}O$ signatures for SIM are a source of uncertainty, because the origin and isotopic value of the ice may be unrelated to the underlying water column, due to differential transport patterns [*Östlund and Hut*, 1984]. Conditions encountered in the Arctic could theoretically produce $\delta^{18}O$ fractionations between 1.5 and 2.7‰ [*Macdonald et al.*, 1999b; *Ekwurzel et al.*, 2001]. In this study, the $\delta^{18}O$ of SIM was set to −2.0‰, in accordance with results of previous studies, to represent value of sea ice in the Canada Basin [*Eicken et al.*, 2002; *Macdonald et al.*, 2002; *Yamamoto-Kawai et al.*, 2009]. The salinity and TA assigned to the SIM are averages taken from two studies performed on first-year sea ice in Franklin Bay during the CASES expedition [*Rysgaard et al.*, 2007; *Miller et al.*, 2011]. The average salinity and TA in sea ice were 4.7 ± 0.5 and 415 ± 35 μmol kg^{-1}, respectively (Table 2).

[34] The properties of the PML also vary seasonally, and again it is difficult to assign set values to the tracers. In summer, the salinity, TA and $\delta^{18}O$ of the PML decrease as a result of freshwater inputs by MW and SIM. During winter, sea ice formation leads to brine rejection and simultaneously, an increase in salinity and TA and a decrease in $\delta^{18}O$, all of which strongly impact the PML properties. To account for the effect of seasonal variability, we defined the winter PML as the water mass located at the bottom of the mixed layer, with the highest salinity (32.0 ± 0.1), TA (2256 ± 12 μmol kg^{-1}) and $\delta^{18}O$ (-2.5 ± 0.2‰) observed during the winter. Hence, the effect of brine rejection generated by ice formation is included in our definition of the winter PML.

[35] The properties of the UHW and ATW were determined by averaging our data at given salinities of 33.1 ± 0.1 and 34.82 ± 0.02, respectively. Our TA and $\delta^{18}O$ measurements at a salinity of 33.1 ± 0.1, give averages for TA of 2283 ± 8 μmol kg^{-1} and for $\delta^{18}O$ of -1.6 ± 0.1‰. In the same study area, *Macdonald et al.* [1989] used a $\delta^{18}O$ signature of −1.1‰ for the UHW with a possible range of −1.1 to −1.8‰. Our $\delta^{18}O$ measurements are also in good agreement with the $\delta^{18}O$ data reported by *Melling and Moore* [1995] for the Beaufort Sea shelf. However, the $\delta^{18}O$ for the UHW in the Beaufort Sea is slightly lower (by 0.5‰) than that for the UHW in the Bering Strait and Chukchi Sea (−1.1‰) [*Cooper et al.*, 1997; *Ekwurzel et al.*, 2001; *Macdonald et al.*, 2002]. One possible explanation for the $\delta^{18}O$ difference is that the UHW contains more meteoric water in the Beaufort Sea than in the Chukchi Sea. This difference also implies that the UHW in the Beaufort Sea carries more negative SIM (i.e., sea ice brine), to balance out the salinity and keep it at 33.1. For the ATW, we measured a TA value of 2297 ± 6 μmol kg^{-1} and a $\delta^{18}O$ signature of 0.27 ± 0.1‰. The chemical properties of Canada Basin deep water (CBDW) are also given in Table 2, but this water mass is not considered further in this study.

4.2. The Combined Use of Salinity, TA, and $\delta^{18}O$ as Tracers of Freshwater

[36] The combined use of salinity, TA and $\delta^{18}O$ as tracers of freshwater inputs to the Arctic Ocean provides a distinct fingerprint of MW and SIM and their interactions with winter PML, UHW and ATW. To our knowledge, the only other study to use $\delta^{18}O$ and TA to distinguish MW and SIM was that by *Yamamoto-Kawai et al.* [2005]. These authors demonstrated that TA can be a useful tracer of freshwater and brine inputs to the Arctic Ocean, and they combined salinity-$\delta^{18}O$ and salinity-TA relationships to estimate the spatial and temporal freshwater and brine distribution in the whole Arctic Ocean. However, they excluded all data from samples shallower than 50 m depth to avoid strong seasonal variability. Here, we have considered all samples, including surface waters and those collected on the shelf and close to the Mackenzie River delta.

[37] Given the range of values recorded along the salinity gradient from the river mouth, $\delta^{18}O$ remains a good tracer to distinguish MW (−18.9‰) from the winter PML (−2.5‰) but is a less powerful tracer to separate SIM (−2.0‰) from the winter PML. The efficiency of a given tracer (i.e., TA or $\delta^{18}O$) in decomposing a water mass into its constituent parts is a matter of the signal-to-noise ratio. The efficiency-gradient (EG) of a tracer, along the salinity gradient between 2 end-members (i.e., MW-PML or SIM-PML), is estimated by the following equation:

$$EG = (X_{EM} - X_{PML})/(S_{EM} - S_{PML}), \quad (5)$$

where X is the value of the tracer in the corresponding end-member, EM (MW or SIM). Assuming an ideal mixing between MW and PML, the efficiency gradients of TA and $\delta^{18}O$ are 19.9 μmol kg^{-1} psu^{-1} and 0.51‰ psu^{-1}, respectively. The efficiency gradients of TA and $\delta^{18}O$ for a mix of SIM with PML are 67.4 μmol kg^{-1} psu^{-1} and 0.02‰ psu^{-1}, respectively. Note that in the latter case, the efficiency-gradient of $\delta^{18}O$ is below the precision of our $\delta^{18}O$ measurements (0.05‰), making it a particularly poor tracer for separating SIM and PML waters. Thus, the combination of salinity, TA and $\delta^{18}O$ is a powerful tool to distinguish all the freshwater fractions.

4.3. Seasonal Variation in Water Mass Distribution

[38] Here, we examine the water mass distribution in the southeastern Beaufort Sea with respect to the carbonate system over the three seasonal periods. The description that follows is admittedly a simplification, but it illustrates the variability of carbonate parameters and $\delta^{18}O$ in response to seasonal events such as the spring freshet, ice break-up and freezeup in the study area. Using the water mass properties in Table 2, we applied the OMP analysis to derive the temporal variations of water mass distributions, in autumn and summer, along 5 transects: the Mackenzie and Kugmallit canyons, 2 SW-NE transects across the Cape Bathurst Polynya, and a NW-SE transect from the Beaufort Sea into Amundsen Gulf (Figure 1). We used the same method to derive the water mass distributions during the over-wintering

period in Franklin Bay. Note that we reproduce here only the results for the Kugmallit Canyon transect and for the winter station. Results for the other transects are reproduced in the auxiliary material.[1]

[39] In autumn 2003, the Mackenzie River flow fell below 10,000 m^3 s^{-1} (Figure 3). Hence, the influence of the Mackenzie River plume ($fCO_{2\text{-}SW}$ > 500 μatm) was relatively small (less than 15%) along the Kugmallit Canyon and limited to the top 10 m of the inner shelf (Figure 7). With the exception of a small residual lens, MW was not detected beyond the shelf break. The relative contribution of SIM reached 20% in the first 20 m and decreased to 5% at 30 m depth. In contrast to MW, SIM was observed beyond the shelf break, i.e., close to the ice pack, in association with low fCO_2-sw (282 $\pm$ 12 μatm, n = 32). On the shelf, the PML extended from 20 to 50 m depth whereas the UHW was found deeper, between 120 and 180 m depth, off the shelf in the Beaufort Sea. The ATW predominated from 200 to 800 m depth whereas, at greater depths, the Canada Basin deep water contributed about 50% to the water mass (data not shown). The overall water mass distributions agree with the previous description by *Macdonald et al.* [1989].

[40] At the same period, the relative contribution of MW was nearly the same (8 $\pm$ 2%) in the Cape Bathurst Polynya as on the eastern part of the Mackenzie Shelf (see auxiliary material). Our results suggest an export of MW from the Mackenzie Shelf to the Amundsen Gulf as previously observed by the disposition of the Mackenzie plume when winds were mostly from the southwest to the northwest [*Macdonald and Yu*, 2006]. Results from a coupled ice-ocean general circulation model indicate that most of the Mackenzie River Water flows out of the Beaufort Sea relatively quickly, probably through the Canadian Arctic Archipelago [*Karcher and Oberhuber*, 2002]. However, some studies showed that the Mackenzie River plume can move northward across the western shelf and once reaching the interior ocean, track westward in the Beaufort Gyre [*Macdonald et al.*, 1999a, 2002]. On the other hand, the MW fractions we found in the Cape Bathurst Polynya could also be residual input from the Husky or Horton Rivers, located in Franklin Bay. The Cape Bathurst Polynya is a site of enhanced air-sea heat exchange, and thus, SIM contributes 10%, on average, of the SML. Moreover, it is not surprising to observe a high proportion of SIM in the autumn, as Arctic sea ice usually reaches its lowest annual extent in mid-September [*Stroeve et al.*, 2005; *Howell et al.*, 2009]. At that time, the surface mixed layer of the Cape Bathurst Polynya was undersatured (298 $\pm$ 28 μatm, n = 105) with respect to atmospheric CO_2, and therefore acts as a net sink of CO_2 [*Mucci et al.*, 2010].

[41] The UHW is located between 120 and 180 m depth everywhere along the Cape Bathurst Polynya transects (auxiliary material). The UHW is, therefore, likely exported eastward from the Beaufort Sea to the Amundsen Gulf, and it shoals toward the Canadian Arctic Archipelago, as supported by field observations [*Bidleman et al.*, 2007; *Shadwick et al.*, 2009]. In autumn and in the vicinity of Cape Bathurst, the UHW accounted for more than 50% of the water mass at 50 m depth, which is consistent with deep water upwelling along the shelf [*Williams and Carmack*, 2008; *Pickart et al.*, 2009; *Mucci et al.*, 2010]. Accordingly, the ATW was found at shallower depths right off Cape Bathurst than in the other parts of the polynya.

[42] In summer 2004, a sharp pycnocline developed in the surface waters of the Mackenzie Shelf due to freshwater input and increasing sea surface temperature. At the beginning of what we have termed the summer period, the Mackenzie River flow was greater than 20,000 m^3 s^{-1}, and it was still higher than 10,000 m^3 s^{-1} at the end of our study (Figure 3). The influence of that high Mackenzie outflow was evident in the upper 10 m along the Mackenzie Canyon and beyond the shelf break (auxiliary material). Conversely, the Mackenzie plume was detected only on the inner shelf along Kugmallit Canyon. Offshore, along the Mackenzie Canyon, SIM contributed 15% of surface water down to 20 m depth. During the summer, with ice-melt and inputs from the Mackenzie River, a 10 to 20 m layer of freshwater completely occupied the shelf. As a consequence, sea surface fCO_2-sw decreased rapidly from 550 μatm at the Mackenzie River mouth to 250 μatm offshore. In contrast, the contributions of MW and SIM were smaller in the Cape Bathurst Polynya. River runoff accounted for less than 10% of the SML whereas SIM contributed, locally, up to 15%. These percentages are relatively small, but they could account for a large volume of freshwater. If we assume that the surface of the Cape Bathurst Polynya could range between 10,000 and 60,000 km^2, depending on ice cover, with a 3 and 5 m standing stock of MW and SIM, respectively, distributed over that surface area, we estimate freshwater inputs from these fractions of 30 to 180 km^3 for MW and 50 to 300 km^3 for SIM.

[43] As observed in the autumn, the UHW extends from the interior ocean onto the outer shelf from 120 to 180 m depth (Figure 7). Relatively high fractions of UHW were also found at 50 m depth along the Mackenzie Canyon. The Mackenzie and Kugmallit Canyons, as well as Cape Bathurst, are all recognized sites of enhanced shelf-break upwelling caused by wind- and ice-driven ocean surface stresses [*Williams et al.*, 2006, 2008; *Williams and Carmack*, 2008]. During wind-driven upwelling, the UHW can mix with the PML, and the associated inputs of nutrients can support relatively high primary production on the outer Mackenzie Shelf and at the shelf-break [*Macdonald et al.*, 1987; *Carmack et al.*, 2004]. Below 200 m depth, ATW was always the prevailing water mass.

4.4. A Winter Time Series in Franklin Bay

[44] The water mass distribution in Franklin Bay over the winter is shown in Figure 8. In early December 2003, the relative contributions of MW and SIM to the SML were very low (less than 8%) and close to the detection limits of the OMP analysis. In late December 2003, contributions of MW and SIM became insignificant after the passage of an upwelling eddy-like feature [*Tremblay et al.*, 2008]. Despite limited sampling at that time, we still observed a significant increase in TIC (from 2050 to 2190 μmol kg^{-1}) and $fCO_{2\text{-}SW}$ (from 367 μatm to 465 μatm) in the mixed layer. The higher resolution temperature and salinity data clearly document the upwelling of the UHW to 50 m depth (Figure 6). During the winter, brine rejection can induce eddies that strongly impact the vertical structure of the halocline [*Mathis et al.*, 2007; *Spall et al.*, 2008; *Timmermans et al.*, 2008]. Eddies impact

[1] Auxiliary materials are available in the HTML. doi:10.1029/2011JC007299.

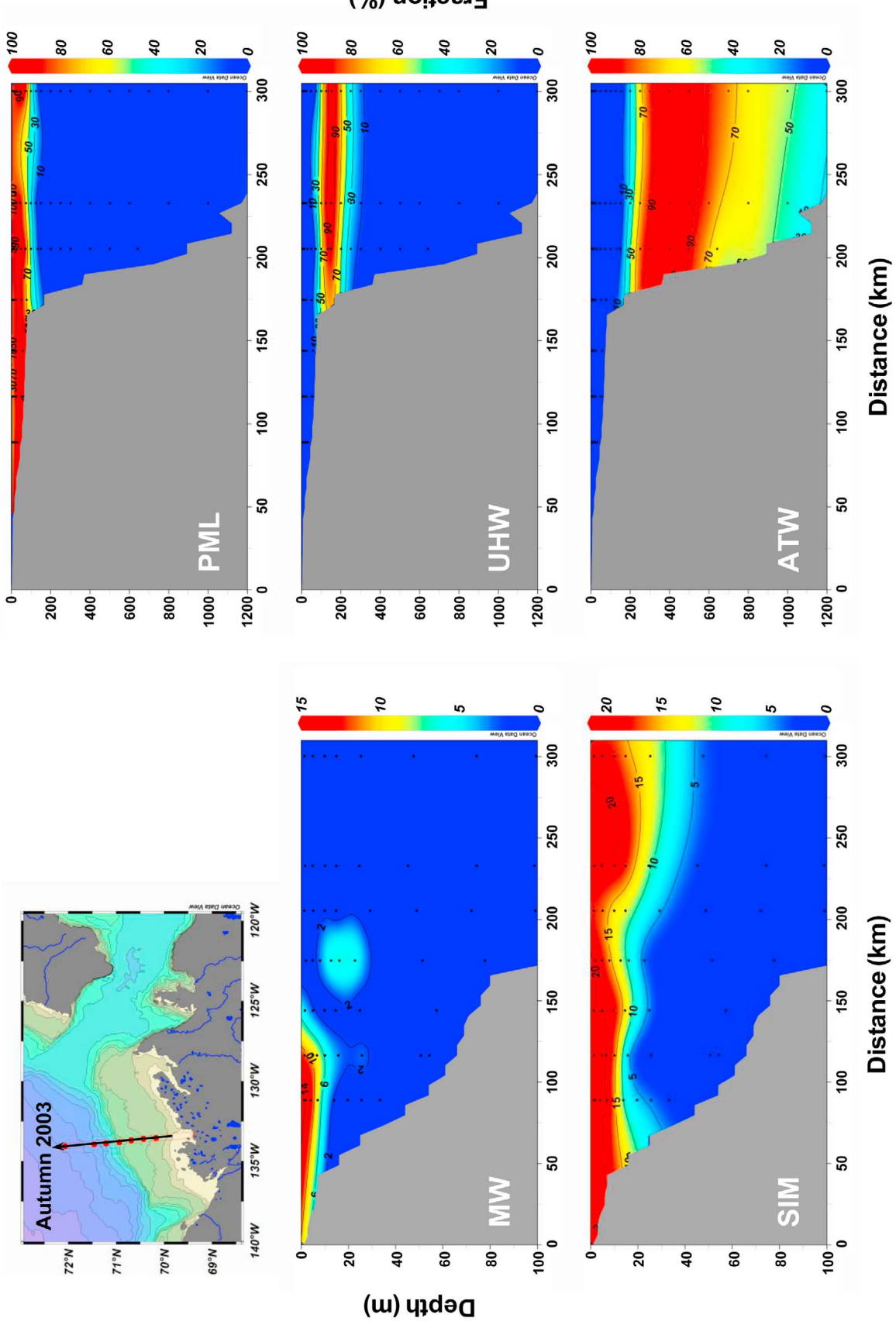

Figure 7. Example of water mass distribution (%) along Kugmalitt canyon in autumn 2003. The water masses are: Mackenzie water (MW), sea ice melt (SIM), winter polar mixed layer (PML), upper halocline water (UHW), and Atlantic water (ATW).

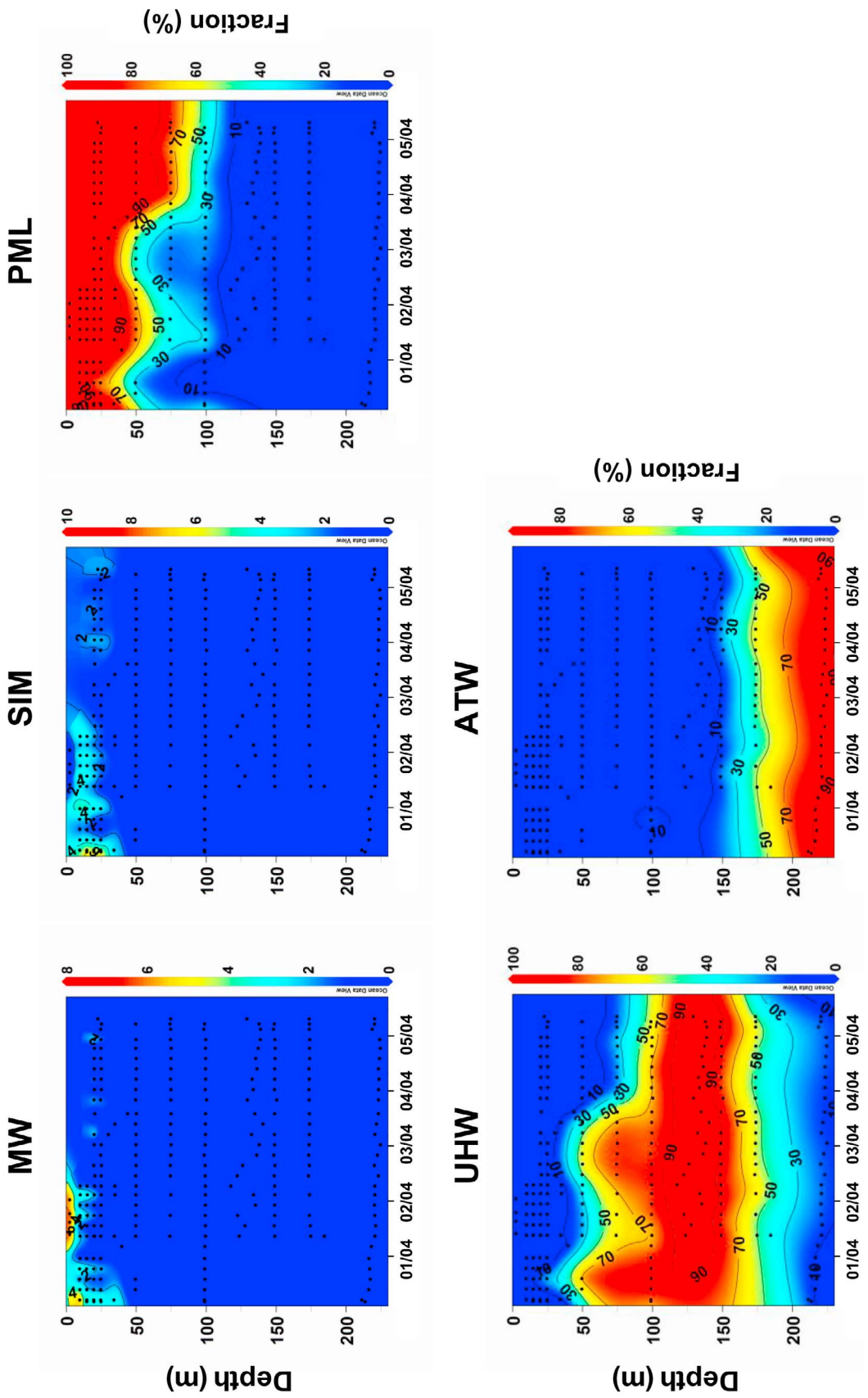

Figure 8. Variability of water mass distribution (%) in Franklin Bay during winter-spring 2003–2004. The water masses are: Mackenzie water (MW), sea ice melt (SIM), winter polar mixed layer (PML), upper halocline water (UHW), and Atlantic water (ATW).

mixing and vertical heat transfer in the halocline and, by trapping and transporting water, affect the lateral transport of heat, salt and other water properties within the Canada Basin. The chemical properties of the SML and the halocline were strongly affected by the passage of an eddy in Franklin Bay (22 December 2003). The $\delta^{18}O$ increases from −3.85‰ to −2.33‰ in the SML (Figure 6) and clearly indicates that vertical mixing, as well as possibly advection from offshore, occurred during our study.

[45] Throughout the winter, the addition of salt by brine rejection from sea ice increased the density of the SML. As a result, the newly formed winter PML became denser, and its thickness in Franklin Bay reached a maximum depth of 70 m in late April 2004. Similarly, the upper limit of the UHW layer shifted from 50 m to 100 m depth between December and April. Year after year, the mixing process induced by brine rejection increases the density of the winter PML that can ultimately feed the UHW [*Melling*, 1993; *Rudels et al.*, 1996]. In contrast, the depth of the deep pycnocline (about 180 m) remained stable over the winter, and significant amounts of ATW (greater than 80%) were always found below 200 m depth.

5. Conclusion

[46] The Arctic Ocean is prone to rapid transformations, such as changes in sea ice melt and freezing rates, increased freshwater input to the shelves due to higher riverine discharge, changing carbon and sediment fluxes due to coastal erosion and permafrost thawing, altering freshwater transport patterns on the shelf seas, and modifications to the inflow of water masses from the Pacific and Atlantic Oceans, not to mention the associated, complex ecosystem changes. The identification of freshwater inputs and seawater masses is crucial for our understanding of change in the Arctic Ocean. In this study, water mass distributions in the southeastern Beaufort Sea were examined using salinity, TA and $\delta^{18}O$ as tracers of freshwater inputs in an optimum multiparameter analysis. The results of the water mass distribution depend on the assigned end-member properties, but the overall distributions we have derived are in agreement with previous studies [*Macdonald et al.*, 1989, 2002; *Yamamoto-Kawai et al.*, 2005, 2008]. The water mass distribution analysis performed in this study shows the following:

[47] 1. The influence of the Mackenzie water ($fCO_{2\text{-}SW}$ > 500 μatm) was relatively small in the southeastern Beaufort Sea and significant fractions of MW were only observed on the inner Mackenzie Shelf in summer 2004.

[48] 2. The contribution of SIM ($fCO_{2\text{-}SW}$ < 300 μatm) to the mixed layer reached 30% close to the ice pack in autumn. River runoff and sea ice meltwater occurred concurrently, and both mix with the PML.

[49] 3. When sea ice forms, brine rejection modifies the properties of the SML and contributes to the newly formed winter PML. The density of the winter PML increases through the winter, and the depth of the winter PML can reach a maximum of 70 m in late April 2004.

[50] 4. The UHW, located between 120 and 180 m depth, is exported from the Beaufort Sea to the Canadian Arctic Archipelago through Cape Bathurst Polynya. As the UHW is supersaturated ($fCO_{2\text{-}SW}$ > 600 μatm) with respect to atmospheric CO_2, the occurrence and magnitude of upwelling events and their effects on the carbonate system in the Canadian Arctic Archipelago must be addressed, as we try to predict the future role of the Arctic Ocean in the absorption or rejection of atmospheric CO_2.

[51] **Acknowledgments.** We thank the officers and crew of the CCGS *Amundsen* for their support and dedication to the CASES expedition. We are indebted to Constance Guignard, Nes Sutherland, Pascale Collin, Simon Bélanger, Jens Ehn, Mike Arychuk and Owen Owens for their care and perseverance in collecting and analyzing the TA, TIC and pH samples at sea. Thanks must go to the CTD data acquisition group for these basic but critical measurements and the calibration of the various probes. Most of the plots and maps in this study were created with the ODV Software [*Schlitzer*, 2009]. We also thank A. Proshutinsky and two anonymous reviewers who provided constructive comments that helped to improve our manuscript. This study was funded through the CASES (Canadian Arctic Shelf Exchange Study) NSERC network (Natural Sciences and Engineering Research Council of Canada) and a Canadian Fund for Innovation grant to support the upgrade and operation of the CCGS Amundsen. Additional financial contributions were provided by the Canadian Coast Guard, the Strategic Science Fund of the Department of Fisheries and Oceans Canada, and NSERC Discovery grants to A. Mucci and Y. Gratton.

References

Aagaard, K., L. K. Coachman, and E. Carmack (1981), On the halocline of the Arctic Ocean, *Deep Sea Res., Part A*, *28*(6), 529–545, doi:10.1016/0198-0149(81)90115-1.

Alkire, M. B., and J. H. Trefry (2006), Transport of spring floodwater from rivers under ice to the Alaskan Beaufort Sea, *J. Geophys. Res.*, *111*, C12008, doi:10.1029/2005JC003446.

Anderson, L. G., and S. Kaltin (2001), Carbon fluxes in the Arctic Ocean—Potential impact by climate change, *Polar Res.*, *20*(2), 225–232, doi:10.1111/j.1751-8369.2001.tb00060.x.

Anderson, L. G., D. Dyrssen, and E. P. Jones (1990), An assessment of the transport of atmospheric CO_2 into the Arctic Ocean, *J. Geophys. Res.*, *95*(C2), 1703–1711, doi:10.1029/JC095iC02p01703.

Anderson, L. G., E. Falck, E. P. Jones, S. Jutterström, and J. H. Swift (2004a), Enhanced uptake of atmospheric CO_2 during freezing of seawater: A field study in Storfjorden, Svalbard, *J. Geophys. Res.*, *109*, C06004, doi:10.1029/2003JC002120.

Anderson, L. G., S. Jutterström, S. Kaltin, E. P. Jones, and G. Björk (2004b), Variability in river runoff distribution in the Eurasian Basin of the Arctic Ocean, *J. Geophys. Res.*, *109*, C01016, doi:10.1029/2003JC001773.

Arrigo, K. R., and G. L. van Dijken (2004), Annual cycles of sea ice and phytoplankton in Cape Bathurst Polynya, southeastern Beaufort Sea, Canadian Arctic, *Geophys. Res. Lett.*, *31*, L08304, doi:10.1029/2003GL018978.

Arrigo, K. R., G. van Dijken, and S. Pabi (2008), Impact of a shrinking Arctic ice cover on marine primary production, *Geophys. Res. Lett.*, *35*, L19603, doi:10.1029/2008GL035028.

Barber, D. G., and J. M. Hanesiak (2004), Meteorological forcing of sea ice concentrations in the southern Beaufort Sea over the period 1979 to 2000, *J. Geophys. Res.*, *109*, C06014, doi:10.1029/2003JC002027.

Bates, N. R., and J. T. Mathis (2009), The Arctic Ocean marine carbon cycle: Evaluation of air-sea CO_2 exchanges, ocean acidification impacts and potential feedbacks, *Biogeosciences*, *6*, 2433–2459, doi:10.5194/bg-6-2433-2009.

Bauch, D., H. Erlenkeuser, and N. Andersen (2005), Water mass processes on Arctic shelves as revealed from $\delta^{18}O$ of H_2O, *Global Planet. Change*, *48*(1–3), 165–174, doi:10.1016/j.gloplacha.2004.12.011.

Benner, R., B. Benitez-Nelson, K. Kaiser, and R. M. W. Amon (2004), Export of young terrigenous dissolved organic carbon from rivers to the Arctic Ocean, *Geophys. Res. Lett.*, *31*, L05305, doi:10.1029/2003GL019251.

Bidleman, T. F., H. Kylin, L. M. Jantunen, P. A. Helm, and R. W. Macdonald (2007), Hexachlorocyclohexanes (HCHs) in the Canadian Archipelago. Part 1. Spatial distribution and pathways of alpha-, beta- and gamma-HCHs in surface water, *Environ. Sci. Technol.*, *41*, 2688–2695, doi:10.1021/es062375b.

Byrne, R. H. (1987), Standardization of standard buffers by visible spectrometry, *Anal. Chem.*, *59*, 1479–1481, doi:10.1021/ac00137a025.

Cai, W.-J., et al. (2010), Decrease in the CO_2 uptake capacity in an ice-free Arctic Ocean basin, *Science*, *329*, 556–559, doi:10.1126/science.1189338.

Carmack, E. C., and R. W. Macdonald (2002), Oceanography of the Canadian Shelf of the Beaufort Sea: A setting for marine life, *Arctic*, *55*, suppl. 1, 29–45.

Carmack, E. C., R. W. MacDonald, and J. E. Papadakis (1989), Water mass structure and boundaries in the Mackenzie Shelf estuary, *J. Geophys. Res.*, *94*(C12), 18,043–18,055, doi:10.1029/JC094iC12p18043.

Carmack, E. C., R. W. Macdonald, and S. Jasper (2004), Phytoplankton productivity on the Canadian Shelf of the Beaufort Sea, *Mar. Ecol. Prog. Ser.*, *277*, 37–50, doi:10.3354/meps277037.

Clayton, T. D., and R. H. Byrne (1993), Spectrophotometric seawater pH measurements: Total hydrogen ion concentration scale calibration of m-cresol purple and at-sea results, *Deep Sea Res., Part I*, *40*, 2115–2129, doi:10.1016/0967-0637(93)90048-8.

Cooper, L. W., T. E. Whitledge, J. M. Grebmeier, and T. Weingartner (1997), The nutrient, salinity, and stable oxygen isotope composition of Bering and Chukchi Seas waters in and near the Bering Strait, *J. Geophys. Res.*, *102*(C6), 12,563–12,573, doi:10.1029/97JC00015.

Cooper, L. W., R. Benner, J. W. McClelland, B. J. Peterson, R. M. Holmes, P. A. Raymond, D. A. Hansell, J. M. Grebmeier, and L. A. Codispoti (2005), Linkages among runoff, dissolved organic carbon, and the stable oxygen isotope composition of seawater and other water mass indicators in the Arctic Ocean, *J. Geophys. Res.*, *110*, G02013, doi:10.1029/2005JG000031.

Cooper, L. W., J. W. McClelland, R. M. Holmes, P. A. Raymond, J. J. Gibson, C. K. Guay, and B. J. Peterson (2008), Flow-weighted values of runoff tracers ($\delta^{18}O$, DOC, Ba, alkalinity) from the six largest Arctic rivers, *Geophys. Res. Lett.*, *35*, L18606, doi:10.1029/2008GL035007.

Delille, B., B. Jourdain, A. V. Borges, J.-L. Tison, and D. Delille (2007), Biogas (CO_2, O_2, dimethylsulfide) dynamics in spring Antarctic fast ice, *Limnol. Oceanogr.*, *52*(4), 1367–1379, doi:10.4319/lo.2007.52.4.1367.

Dickson, A. G. (1990), Standard potential of the reaction: AgCl(s) + $1/2H_2(g)$ = Ag(s) + HCl(aq), and the standard acidity constant of the ion HSO_4^- in synthetic sea water from 273.15 to 318.15 K, *J. Chem. Thermodyn.*, *22*(2), 113–127, doi:10.1016/0021-9614(90)90074-Z.

Dickson, A. G., and C. Goyet (Eds.) (1994), Handbook of methods for the analysis of the various parameters of the carbon dioxide system in sea water, version 2, *Rep. ORNL/CDIAC-74*, Dep. of Energy, Washington, D. C.

Dickson, A. G., and F. J. Millero (1987), A comparison of the equilibrium constants for the dissociation of carbonic acid in seawater media, *Deep Sea Res., Part A*, *34*(10), 1733–1743, doi:10.1016/0198-0149(87)90021-5.

Eicken, H., H. R. Krouse, D. Kadko, and D. K. Perovich (2002), Tracer studies of pathways and rates of meltwater transport through Arctic summer sea ice, *J. Geophys. Res.*, *107*(C10), 8046, doi:10.1029/2000JC000583.

Ekwurzel, B., P. Schlosser, R. A. Mortlock, R. G. Fairbanks, and J. H. Swift (2001), River runoff, sea ice meltwater, and Pacific water distribution and mean residence times in the Arctic Ocean, *J. Geophys. Res.*, *106*(C5), 9075–9092, doi:10.1029/1999JC000024.

Else, B. G., T. N. Papakyriakou, R. J. Galley, W. M. Drennan, L. A. Miller, and H. Thomas (2011), Wintertime CO_2 fluxes in an Arctic polynya using eddy covariance: Evidence for enhanced air-sea gas transfer during ice formation, *J. Geophys. Res.*, *116*, C00G03, doi:10.1029/2010JC006760.

Epstein, S., and T. Mayeda (1953), Variation of O^{18} content of waters from natural sources, *Geochim. Cosmochim. Acta*, *4*(5), 213–224, doi:10.1016/0016-7037(53)90051-9.

Fransson, A., M. Chierici, and Y. Nojiri (2009), New insights into the spatial variability of the surface water carbon dioxide in varying sea ice conditions in the Arctic Ocean, *Cont. Shelf Res.*, *29*(10), 1317–1328, doi:10.1016/j.csr.2009.03.008.

Gibson, J. A. E., and T. W. Trull (1999), Annual cycle of fCO_2 under sea-ice and in open water in Prydz Bay, East Antarctica, *Mar. Chem.*, *66*(3–4), 187–200, doi:10.1016/S0304-4203(99)00040-7.

Grasshoff, K., M. Ehrhardt, and K. Kremling (Eds.) (1983), *Methods of Seawater Analysis*, 2nd edition, 420 pp., Verlag Chemie, Berlin.

Gratton, Y., P. Galbraith, L. Prieur, M. Kamali Nezhad, and C. Bélanger (2006), Water column variability at the CASES winter station (Franklin Bay, Canada), paper presented at 2006 General Meeting, Can. Arct. Shelf Exch. Study, Winnipeg, Manit., Canada, 13–16 Feb.

Guay, C. K., and K. K. Falkner (1997), Barium as a tracer of Arctic halocline and river waters, *Deep Sea Res., Part II*, *44*(8), 1543–1569, doi:10.1016/S0967-0645(97)00066-0.

Guay, C. K. H., F. A. McLaughlin, and M. Yamamoto-Kawai (2009), Differentiating fluvial components of upper Canada Basin waters on the basis of measurements of dissolved barium combined with other physical and chemical tracers, *J. Geophys. Res.*, *114*, C00A09, doi:10.1029/2008JC005099.

Guo, L., C.-L. Ping, and R. W. Macdonald (2007), Mobilization pathways of organic carbon from permafrost to arctic rivers in a changing climate, *Geophys. Res. Lett.*, *34*, L13603, doi:10.1029/2007GL030689.

Howell, S. E. L., C. R. Duguay, and T. Markus (2009), Sea ice conditions and melt season duration variability within the Canadian Arctic Archipelago: 1979–2008, *Geophys. Res. Lett.*, *36*, L10502, doi:10.1029/2009GL037681.

Intergovernmental Panel on Climate Change (2008), *Climate Change 2007: Synthesis Report. Contribution of Working Groups I, II and III to the Fourth Assessment Report of the Intergovernmental Panel on Climate Change*, edited by Core Writing Team et al., 104 pp., Geneva, Switzerland. [Available at http://www.ipcc.ch/publications_and_data/ar4/syr/en/contents.html.]

Jeansson, E., S. Jutterström, B. Rudels, L. G. Anderson, K. A. Olsson, E. P. Jones, W. M. Smethie Jr., and J. H. Swift (2008), Sources to the East Greenland Current and its contribution to the Denmark Strait Overflow, *Prog. Oceanogr.*, *78*(1), 12–28, doi:10.1016/j.pocean.2007.08.031.

Johnson, K. M., K. D. Wills, D. B. Butler, W. K. Johnson, and C. S. Wong (1993), Coulometric total carbon dioxide analysis for marine studies: Maximizing the performance of an automated gas extraction system and coulometric detector, *Mar. Chem.*, *44*(2–4), 167–187, doi:10.1016/0304-4203(93)90201-X.

Jones, E. P., and L. G. Anderson (1986), On the origin of the chemical properties of the Arctic Ocean halocline, *J. Geophys. Res.*, *91*(C9), 10,759–10,767, doi:10.1029/JC091iC09p10759.

Jones, E. P., and A. R. Coote (1981), Oceanic CO_2 produced by the precipitation of $CaCO_3$ from brines in sea ice, *J. Geophys. Res.*, *86*(C11), 11,041–11,043, doi:10.1029/JC086iC11p11041.

Jones, E. P., L. G. Anderson, and J. H. Swift (1998), Distribution of Atlantic and Pacific waters in the upper Arctic Ocean: Implications for circulation, *Geophys. Res. Lett.*, *25*, 765–768, doi:10.1029/98GL00464.

Jones, E. P., J. H. Swift, L. G. Anderson, M. Lipizer, G. Civitarese, K. K. Falkner, G. Kattner, and F. McLaughlin (2003), Tracing Pacific water in the North Atlantic Ocean, *J. Geophys. Res.*, *108*(C4), 3116, doi:10.1029/2001JC001141.

Jones, E. P., L. G. Anderson, S. Jutterström, L. Mintrop, and J. H. Swift (2008), Pacific freshwater, river water and sea ice meltwater across Arctic Ocean basins: Results from the 2005 Beringia Expedition, *J. Geophys. Res.*, *113*, C08012, doi:10.1029/2007JC004124.

Karcher, M. J., and J. M. Oberhuber (2002), Pathways and modification of the upper and intermediate waters of the Arctic Ocean, *J. Geophys. Res.*, *107*(C6), 3049, doi:10.1029/2000JC000530.

Karstensen, J. (2006), OMP (Optimum Multiparameter) Analysis - User Group, http://www.ldeo.columbia.edu/~jkarsten/omp_std/, Lamont-Doherty Earth Obs., Palisades, N. Y.

Karstensen, J., P. Schlosser, D. W. R. Wallace, J. L. Bullister, and J. Blindheim (2005), Water mass transformation in the Greenland Sea during the 1990s, *J. Geophys. Res.*, *110*, C07022, doi:10.1029/2004JC002510.

Keeling, R. F., S. C. Piper, A. F. Bollenbacher, and J. S. Walker (2008), Atmospheric CO_2 Records From Sites in the SIO Air Sampling Network, http://cdiac.ornl.gov/trends/co2/sio-keel.html, Carbon Dioxide Inf. Anal. Cent., Oak Ridge, Tenn.

Krouse, H. R., and J. R. Mackay (1971), Application of $H_2{}^{18}O/H_2{}^{16}O$ abundances to the problem of lateral mixing in the Liard–Mackenzie River system, *Can. J. Earth Sci.*, *8*(9), 1107–1109, doi:10.1139/e71-096.

Leffanue, H., and M. Tomczak (2004), Using OMP analysis to observe temporal variability in water mass distribution, *J. Mar. Syst.*, *48*, 3–14, doi:10.1016/j.jmarsys.2003.07.004.

Lehmann, M., and U. Siegenthaler (1991), Equilibrium oxygen- and hydrogen-isotope fractionation between ice and water, *J. Glaciol.*, *37*(125), 23–26.

Lewis, E., and D. W. R. Wallace (1998), Program developed for CO_2 system calculations, *Rep. ORNL/CDIAC-105*, Carbon Dioxide Inf. Anal. Cent., Oak Ridge Natl. Lab., U.S. Dep. of Energy, Oak Ridge, Tenn. [Available at http://cdiac.esd.ornl.gov/oceans/co2rprt.html.]

Macdonald, R. W., and Y. Yu (2006), The Mackenzie estuary of the Arctic Ocean, in *Estuaries (The Handbook of Environmental Chemistry/Water Pollution)*, edited by P. J. Wangersky, pp. 91–120, Springer, Berlin.

Macdonald, R. W., C. S. Wong, and P. E. Erickson (1987), The distribution of nutrients in the southeastern Beaufort Sea: Implications for water circulation and primary production, *J. Geophys. Res.*, *92*(C3), 2939–2952, doi:10.1029/JC092iC03p02939.

Macdonald, R. W., E. C. Carmack, F. A. McLaughlin, K. Iseki, D. M. Macdonald, and M. C. O'Brien (1989), Composition and modification of water masses in the Mackenzie Shelf estuary, *J. Geophys. Res.*, *94*(C12), 18,057–18,070, doi:10.1029/JC094iC12p18057.

Macdonald, R. W., D. W. Paton, E. C. Carmack, and A. Omstedt (1995), The freshwater budget and under-ice spreading of Mackenzie River water in the Canadian Beaufort Sea based on salinity and $^{18}O/^{16}O$ measurements in water and ice, *J. Geophys. Res.*, *100*(C1), 895–919, doi:10.1029/94JC02700.

Macdonald, R. W., E. C. Carmack, F. A. McLaughlin, K. K. Falkner, and J. H. Swift (1999a), Connections among ice, runoff and atmospheric

forcing in the Beaufort Gyre, *Geophys. Res. Lett.*, *26*(15), 2223–2226, doi:10.1029/1999GL900508.

Macdonald, R. W., E. C. Carmack, and D. W. Paton (1999b), Using the $\delta^{18}O$ composition in landfast ice as a record of arctic estuarine processes, *Mar. Chem.*, *65*(1–2), 3–24, doi:10.1016/S0304-4203(99)00007-9.

Macdonald, R. W., F. A. McLaughlin, and E. C. Carmack (2002), Fresh water and its sources during the SHEBA drift in the Canada Basin of the Arctic Ocean, *Deep Sea Res., Part I*, *49*(10), 1769–1785, doi:10.1016/S0967-0637(02)00097-3.

Mackas, D. L., K. L. Denman, and A. F. Bennett (1987), Least squares multiple tracer analysis of water mass composition, *J. Geophys. Res.*, *92*(C3), 2907–2918, doi:10.1029/JC092iC03p02907.

Mathis, J. T., R. S. Pickart, D. A. Hansell, D. Kadko, and N. R. Bates (2007), Eddy transport of organic carbon and nutrients from the Chukchi Shelf: Impact on the upper halocline of the western Arctic Ocean, *J. Geophys. Res.*, *112*, C05011, doi:10.1029/2006JC003899.

McGuire, A. D., L. G. Anderson, T. R. Christensen, S. Dallimore, L. Guo, D. J. Hayes, M. Heimann, T. D. Lorenson, R. W. Macdonald, and N. Roulet (2009), Sensitivity of the carbon cycle in the Arctic to climate change, *Ecol. Monogr.*, *79*(4), 523–555, doi:10.1890/08-2025.1.

McLaughlin, F., E. C. Carmack, R. W. Macdonald, and J. Bishop (1996), Physical and geochemical properties across the Atlantic/Pacific water mass front in the southern Canadian Basin, *J. Geophys. Res.*, *101*(C1), 1183–1197, doi:10.1029/95JC02634.

McLaughlin, F. A., E. C. Carmack, R. W. Macdonald, H. Melling, J. H. Swift, P. A. Wheeler, B. F. Sherr, and E. B. Sherr (2004), The joint roles of Pacific and Atlantic-origin waters in the Canada Basin, 1997–1998, *Deep Sea Res., Part I*, *51*(1), 107–128, doi:10.1016/j.dsr.2003.09.010.

Mehrbach, C., C. H. Culberson, J. E. Hawley, and R. N. Pytkowicz (1973), Measurement of the apparent dissociation constants of carbonic acid in seawater at atmospheric pressure, *Limnol. Oceanogr.*, *18*, 897–907, doi:10.4319/lo.1973.18.6.0897.

Melling, H. (1993), The formation of a haline shelf front in wintertime in an ice-covered arctic sea, *Cont. Shelf Res.*, *13*(10), 1123–1147, doi:10.1016/0278-4343(93)90045-Y.

Melling, H., and R. M. Moore (1995), Modification of halocline source waters during freezing on the Beaufort Sea shelf: Evidence from oxygen isotopes and dissolved nutrients, *Cont. Shelf Res.*, *15*(1), 89–113, doi:10.1016/0278-4343(94)P1814-R.

Miller, L. A., T. N. Papakyriakou, R. E. Collins, J. W. Deming, J. K. Ehn, R. W. Macdonald, A. Mucci, O. Owens, M. Raudsepp, and N. Sutherland (2011), Carbon dynamics in sea ice: A winter flux time series, *J. Geophys. Res.*, *116*, C02028, doi:10.1029/2009JC006058.

Millero, F. J., J.-Z. Zhang, S. Fiol, S. Sotolongo, R. N. Roy, K. Lee, and S. Mane (1993), The use of buffers to measure the pH of seawater, *Mar. Chem.*, *44*(2–4), 143–152, doi:10.1016/0304-4203(93)90199-X.

Millot, R., J. Gaillardet, B. Dupré, and C. J. Allègre (2003), Northern latitude chemical weathering rates: Clues from the Mackenzie River Basin, Canada, *Geochim. Cosmochim. Acta*, *67*(7), 1305–1329, doi:10.1016/S0016-7037(02)01207-3.

Mucci, A., B. Lansard, L. A. Miller, and T. Papakyriakou (2010), CO_2 fluxes across the air-sea interface in the southeastern Beaufort Sea: Ice-free period, *J. Geophys. Res.*, *115*, C04003, doi:10.1029/2009JC005330.

Mundy, C. J., et al. (2009), Contribution of under-ice primary production to an ice-edge upwelling phytoplankton bloom in the Canadian Beaufort Sea, *Geophys. Res. Lett.*, *36*, L17601, doi:10.1029/2009GL038837.

Newton, R., P. Schlosser, D. G. Martinson, and W. Maslowski (2008), Freshwater distribution in the Arctic Ocean: Simulation with a high-resolution model and model-data comparison, *J. Geophys. Res.*, *113*, C05024, doi:10.1029/2007JC004111.

Nilsen, F., F. Cottier, R. Skogseth, and S. Mattsson (2008), Fjord-shelf exchanges controlled by ice and brine production: The interannual variation of Atlantic water in Isfjorden, Svalbard, *Cont. Shelf Res.*, *28*(14), 1838–1853, doi:10.1016/j.csr.2008.04.015.

Nomura, D., H. Yoshikawa-Inoue, and T. Toyota (2006), The effect of sea-ice growth on air-sea CO_2 flux in a tank experiment, *Tellus, Ser. B*, *58*(5), 418–426, doi:10.1111/j.1600-0889.2006.00204.x.

Östlund, H. G., and G. Hut (1984), Arctic ocean water mass balance from isotope data, *J. Geophys. Res.*, *89*(C4), 6373–6381, doi:10.1029/JC089iC04p06373.

Overpeck, J. T., et al. (2005), Arctic system on trajectory to new, seasonally ice-free state, *Eos Trans. AGU*, *86*(34), 309, 312–313, doi:10.1029/2005EO340001.

Papadimitriou, S., H. Kennedy, G. Kattner, G. S. Dieckmann, and D. N. Thomas (2004), Experimental evidence for carbonate precipitation and CO_2 degassing during sea ice formation, *Geochim. Cosmochim. Acta*, *68*(8), 1749–1761, doi:10.1016/j.gca.2003.07.004.

Pickart, R. S. (2004), Shelfbreak circulation in the Alaskan Beaufort Sea: Mean structure and variability, *J. Geophys. Res.*, *109*, C04024, doi:10.1029/2003JC001912.

Pickart, R. S., G. W. K. Moore, D. J. Torres, P. S. Fratantoni, R. A. Goldsmith, and J. Yang (2009), Upwelling on the continental slope of the Alaskan Beaufort Sea: Storms, ice, and oceanographic response, *J. Geophys. Res.*, *114*, C00A13, doi:10.1029/2008JC005009.

Pipko, I. I., I. P. Semiletov, P. Y. Tishchenko, S. P. Pugach, and J. P. Christensen (2002), Carbonate chemistry dynamics in Bering Strait and the Chukchi Sea, *Prog. Oceanogr.*, *55*(1–2), 77–94, doi:10.1016/S0079-6611(02)00071-X.

Retamal, L., S. Bonilla, and W. F. Vincent (2008), Optical gradients and phytoplankton production in the Mackenzie River and the coastal Beaufort Sea, *Polar Biol.*, *31*(3), 363–379, doi:10.1007/s00300-007-0365-0.

Robert-Baldo, G. L., M. J. Morris, and R. H. Byrne (1985), Spectrophotometric determination of seawater pH using phenol red, *Anal. Chem.*, *57*, 2564–2567, doi:10.1021/ac00290a030.

Rudels, B., L. G. Anderson, and E. P. Jones (1996), Formation and evolution of the surface mixed layer and halocline of the Arctic Ocean, *J. Geophys. Res.*, *101*(C4), 8807–8821, doi:10.1029/96JC00143.

Rudels, B., E. P. Jones, U. Schauer, and P. Eriksson (2004), Atlantic sources of the Arctic Ocean surface and halocline waters, *Polar Res.*, *23*(2), 181–208, doi:10.1111/j.1751-8369.2004.tb00007.x.

Rysgaard, S., R. N. Glud, M. K. Sejr, J. Bendtsen, and P. B. Christensen (2007), Inorganic carbon transport during sea ice growth and decay: A carbon pump in polar seas, *J. Geophys. Res.*, *112*, C03016, doi:10.1029/2006JC003572.

Schlitzer, R. (2009), Ocean Data View, http://odv.awi.de/, Alfred Wegner Inst. for Polar Mar. Res., Bremerhaven, Germany.

Schlosser, P., R. Newton, B. Ekwurzel, S. Khatiwala, R. Mortlock, and R. Fairbanks (2002), Decrease of river runoff in the upper waters of the Eurasian Basin, Arctic Ocean, between 1991 and 1996: Evidence from $d^{18}O$ data, *Geophys. Res. Lett.*, *29*(9), 1289, doi:10.1029/2001GL013135.

Semiletov, I. P., I. I. Pipko, I. Repina, and N. E. Shakhova (2007), Carbonate chemistry dynamics and carbon dioxide fluxes across the atmosphere-ice-water interfaces in the Arctic Ocean: Pacific sector of the Arctic, *J. Mar. Syst.*, *66*(1–4), 204–226, doi:10.1016/j.jmarsys.2006.05.012.

Serreze, M. C., A. P. Barrett, A. G. Slater, R. A. Woodgate, K. Aagaard, R. B. Lammers, M. Steele, R. Moritz, M. Meredith, and C. M. Lee (2006), The large-scale freshwater cycle of the Arctic, *J. Geophys. Res.*, *111*, C11010, doi:10.1029/2005JC003424.

Serreze, M. C., M. M. Holland, and J. Stroeve (2007), Perspective on the Arctic's shrinking sea-ice cover, *Science*, *315*, 1533–1536, doi:10.1126/science.1139426.

Shadwick, E. H., T. Papakyriakou, A. E. F. Prowe, D. Leong, S. A. Moore, and H. Thomas (2009), Carbon cycling in the Arctic Archipelago: The export of Pacific carbon to the North Atlantic, *Biogeosci. Discuss.*, *6*(1), 971–994, doi:10.5194/bgd-6-971-2009.

Shadwick, E. H., et al. (2011a), Seasonal variability of the inorganic carbon system in the Amundsen Gulf region of the southeastern Beaufort Sea, *Limnol. Oceanogr.*, *56*(1), 303–322, doi:10.4319/lo.2011.56.1.0303.

Shadwick, E. H., H. Thomas, Y. Gratton, D. Leong, S. A. Moore, T. Papakyriakou, and A. E. F. Prowe (2011b), Export of Pacific carbon through the Arctic Archipelago to the North Atlantic, *Cont. Shelf Res.*, *31*(7–8), 806–816, doi:10.1016/j.csr.2011.01.014.

Shaw, W. J., T. P. Stanton, M. G. McPhee, J. H. Morison, and D. G. Martinson (2009), Role of the upper ocean in the energy budget of Arctic sea ice during SHEBA, *J. Geophys. Res.*, *114*, C06012, doi:10.1029/2008JC004991.

Shcherbina, A. Y., L. D. Talley, and D. L. Rudnick (2003), Direct observations of North Pacific ventilation: Brine rejection in the Okhotsk Sea, *Science*, *302*(5652), 1952–1955, doi:10.1126/science.1088692.

Sherr, B. F., and E. B. Sherr (2003), Community respiration/production and bacterial activity in the upper water column of the central Arctic Ocean, *Deep Sea Res., Part I*, *50*(4), 529–542, doi:10.1016/S0967-0637(03)00030-X.

Shimada, K., T. Kamoshida, M. Itoh, S. Nishino, E. Carmack, F. McLaughlin, S. Zimmermann, and A. Proshutinsky (2006), Pacific Ocean inflow: Influence on catastrophic reduction of sea ice cover in the Arctic Ocean, *Geophys. Res. Lett.*, *33*, L08605, doi:10.1029/2005GL025624.

Skogseth, R., L. H. Smedsrud, F. Nilsen, and I. Fer (2008), Observations of hydrography and downflow of brine-enriched shelf water in the Storfjorden polynya, Svalbard, *J. Geophys. Res.*, *113*, C08049, doi:10.1029/2007JC004452.

Spall, M., R. S. Pickart, P. Fratantoni, and A. Plueddemann (2008), Western Arctic shelfbreak eddies: Formation and transport, *J. Phys. Oceanogr.*, *38*, 1644–1668, doi:10.1175/2007JPO3829.1.

Stroeve, J. C., M. C. Serreze, F. Fetterer, T. Arbetter, W. Meier, J. Maslanik, and K. Knowles (2005), Tracking the Arctic's shrinking ice cover:

Another extreme September minimum in 2004, *Geophys. Res. Lett.*, *32*, L04501, doi:10.1029/2004GL021810.

Symon, C., et al. (Eds.) (2005), *Arctic Climate Impact Assessment*, 1042 pp., Cambridge Univ. Press, Cambirdge, U. K.

Taylor, J. R., K. K. Falkner, U. Schauer, and M. Meredith (2003), Quantitative considerations of dissolved barium as a tracer in the Arctic Ocean, *J. Geophys. Res.*, *108*(C12), 3374, doi:10.1029/2002JC001635.

Telang, S. A., R. Pocklington, A. S. Naidu, E. A. Romankevich, I. I. Gitelson, and M. I. Gladyshev (1991), Carbon and mineral transport in major North American, Russian Arctic, and Siberian rivers: The St. Lawrence, the Mackenzie, the Yukon, the Arctic Alaskan rivers, the Arctic Basin rivers in the Soviet Union, and the Yenisei, in *Biogeochemistry of Major World Rivers*, edited by E. T. Degens et al., pp. 75–104, John Wiley, London.

Thomas, H., et al. (2011), Barium and carbon fluxes in the Canadian Arctic Archipelago, *J. Geophys. Res.*, *116*, C00G08, doi:10.1029/2011JC007120.

Timmermans, M.-L., J. Toole, A. Proshutinsky, R. Krishfield, and A. Plueddemann (2008), Eddies in the Canada Basin, Arctic Ocean, observed from ice-tethered profilers, *J. Phys. Oceanogr.*, *38*, 133–145, doi:10.1175/2007JPO3782.1.

Tomczak, M., and D. G. B. Large (1989), Optimum multiparameter analysis of mixing in the thermocline of the eastern Indian Ocean, *J. Geophys. Res.*, *94*(C11), 16,141–16,149, doi:10.1029/JC094iC11p16141.

Tremblay, J.-É., K. Simpson, J. Martin, L. Miller, Y. Gratton, D. Barber, and N. M. Price (2008), Vertical stability and the annual dynamics of nutrients and chlorophyll fluorescence in the coastal, southeast Beaufort Sea, *J. Geophys. Res.*, *113*, C07S90, doi:10.1029/2007JC004547.

Vallières, C., L. Retamal, P. Ramlal, C. L. Osburn, and W. F. Vincent (2008), Bacterial production and microbial food web structure in a large arctic river and the coastal Arctic Ocean, *J. Mar. Syst.*, *74*(3–4), 756–773, doi:10.1016/j.jmarsys.2007.12.002.

White, D., et al. (2007), The Arctic freshwater system: Changes and impacts, *J. Geophys. Res.*, *112*, G04S54, doi:10.1029/2006JG000353.

Williams, W. J., and E. C. Carmack (2008), Combined effect of wind-forcing and isobath divergence on upwelling at Cape Bathurst, Beaufort Sea, *J. Mar. Res.*, *66*(5), 645–663, doi:10.1357/002224008787536808.

Williams, W. J., E. C. Carmack, K. Shimada, H. Melling, K. Aagaard, R. W. Macdonald, and R. G. Ingram (2006), Joint effects of wind and ice motion in forcing upwelling in Mackenzie Trough, Beaufort Sea, *Cont. Shelf Res.*, *26*(19), 2352–2366, doi:10.1016/j.csr.2006.06.012.

Williams, W. J., H. Melling, E. C. Carmack, and R. G. Ingram (2008), Kugmallit Valley as a conduit for cross-shelf exchange on the Mackenzie Shelf in the Beaufort Sea, *J. Geophys. Res.*, *113*, C02007, doi:10.1029/2006JC003591.

Woodgate, R. A., K. Aagaard, and T. J. Weingartner (2006), Interannual changes in the Bering Strait fluxes of volume, heat and freshwater between 1991 and 2004, *Geophys. Res. Lett.*, *33*, L15609, doi:10.1029/2006GL026931.

Yamamoto-Kawai, M., N. Tanaka, and S. Pivovarov (2005), Freshwater and brine behaviors in the Arctic Ocean deduced from historical data of δ^{18}O and alkalinity (1929–2002 A.D.), *J. Geophys. Res.*, *110*, C10003, doi:10.1029/2004JC002793.

Yamamoto-Kawai, M., F. A. McLaughlin, E. C. Carmack, S. Nishino, and K. Shimada (2008), Freshwater budget of the Canada Basin, Arctic Ocean, from salinity, δ^{18}O, and nutrients, *J. Geophys. Res.*, *113*, C01007, doi:10.1029/2006JC003858.

Yamamoto-Kawai, M., F. A. McLaughlin, E. C. Carmack, S. Nishino, K. Shimada, and N. Kurita (2009), Surface freshening of the Canada Basin, 2003–2007: River runoff versus sea ice meltwater, *J. Geophys. Res.*, *114*, C00A05, doi:10.1029/2008JC005000.

Yi, Y., J. J. Gibson, J.-F. Hélie, and T. A. Dick (2010), Synoptic and time-series stable isotope surveys of the Mackenzie River from Great Slave Lake to the Arctic Ocean, 2003 to 2006, *J. Hydrol.*, *383*(3–4), 223–232, doi:10.1016/j.jhydrol.2009.12.038.

Y. Gratton, Centre Eau, Terre et Environnement, Institut National de la Recherche Scientifique, 490 de la Couronne, Québec City, QC G1K 9A9, Canada.

B. Lansard, Laboratoire d'Études en Géophysique et Océanographie Spatiales, Observatoire Midi-Pyrénées, 14, Ave. Édouard Belin, F-31400 Toulouse, France. (lansard@legos.obs-mip.fr)

R. W. Macdonald and L. A. Miller, Centre for Ocean Climate Chemistry, Institute of Ocean Sciences, Fisheries and Oceans Canada, PO Box 6000, Sidney, BC V8L 4B2, Canada.

A. Mucci, Department of Earth and Planetary Sciences, McGill University, 3450 University St., Montréal, QC H3A 2A7, Canada.